Summer 2019

Damping in Transient Pressurized Flows

Sahad Salim Elyass Khilqa

Damping in Transient Pressurized Flows

by

Sahad Salim Elyass Khilqa

Bachelor of Science
University of Mosul, 2001

Master of Science
University of Mosul, 2004

Master of Science
University of South Carolina, 2017

Submitted in Partial Fulfillment of the Requirements

for the Degree of Doctor of Philosophy in

Civil Engineering

College of Engineering and Computing

University of South Carolina

2019

Accepted by:

M. Hanif Chaudhry, Major Professor

Jasim Imran, Committee Member

Enrica Viparelli, Committee Member

Jamil Khan, Committee Member

Cheryl L. Addy, Vice Provost and Dean of the Graduate School

Dedication

To my lovely wife, Rasha Jirjees, my children, Matti, Kerlss and John, my parents, Salim Khilqa, and Janet Butrus, and my brothers, Manhal, Firas, Sarmad and Wisam, I dedicate this work to them. This work would not have been completed without their love, support and prayers.

Acknowledgments

I thank the Ministry of Higher Education and Scientific Research in Iraq and the Iraqi Cultural Office at Washington D.C. for their scholarship, which enabled me to conduct this dissertation. Also, I thank Northern Technical University, Engineering Technical College, Department of Building and Constructions Technology at Mosul for their support.

The author deeply thanks Professor M. Hanif Chaudhry, principal advisor of this research, for his invaluable guidance, good advice and strong support during all times and difficulties. I express my thanks and gratitude to the distinguished members of the committee: Dr. Jasim Imran, Dr. Enrica Viparelli, and Dr. Jamil Khan for their suggestions and recommendations. I thank Professor Juan Caicedo and Dr. Mohamed Elkholy for their contribution to complete this research. I thank Dr. John Dickerson for his help with the experimental setup. Last but not the least, I thank my colleague, Mohammed Al-Tofan and the administrative staff in the Civil Engineering Department, Karen Ammarell, Brian Hull, and Jamie Wurdinger.

Abstract

Piping systems are commonly designed to withstand the first transient pressure peak, which is unaffected by dissipation. However, for multiple operations of control equipment, e.g., pump start-up following pump shutdown, load acceptance following load rejection on hydraulic turbines, etc., an accurate prediction of the dissipation of pressure oscillations is needed to determine a suitable time for the second operation. For this purpose, a method is presented to compute the dissipation of pressure oscillations in piping system following a simple procedure used for computing the dissipation of vibrations of bridges and other structures. Similar to structural engineering, this method is simple to apply, does not require simulation of the entire system, is not computationally intensive, and gives reasonable results for practical applications for a complex phenomenon mechanics of which is not well understood. An empirical equation for the damping ratio is developed by using the dimensional analysis and by nonlinear regression. Comparisons of the computed and experimental results for 17 tests conducted in laboratories all over the globe show good agreement. It is found that the damping ratio increases with increase in Reynolds number or Mach number but decreases with diameter to length ratio of the pipeline. The uncertainty of the model to determine the damping of pressure head oscillations following a sudden valve closure in a simple piping system in pressurized closed conduit using Bayesian inference is quantified. The joint probability density of the model parameter is estimated based on experimental results published in the literature as well as from experiments performed at the University of South Carolina. A Markov Chain of the posterior joint distribution of the model parameters is calculated and used to predict the pressure

head oscillations. The prediction is based on a probabilistic analysis to estimate an interval of pressure as a function of time, rather than estimating a single point if simple regression analysis is done. The 95% high posterior density of the damping ratio is found to range between 1% to 6%. Uncertainty analysis shows that the model predicts the value of the damping ratio successfully.

Table of Contents

List of Tables

List of Figures

Chapter 1

Introduction

1.1 General

Whenever the flow is disturbed in the pressurized flows in closed conduits, waves are generated that propagate back and forth in the piping system until dissipated due to energy losses. This phenomenon, called waterhammer or hydraulic transient, is unsteady nonuniform. Transient flow is the intermediate state flow when the flow conditions are changing from one initial steady state to another steady state. In waterhammer, kinetic energy transforms into pressure energy. This energy could be significant, and if it is not controlled properly, it may damage the piping system, pumps or regulators.

To illustrate the risk of transient event occurring in a piping system, let's assume the following in a piping system: Initial flow velocity, $V = 1$ m/s, length of the pipe, $L = 1000$ m, cross-sectional area , $A = 1$ m^2, and fluid mass density = 1000 kg/m^3. By applying Newton's second law, i.e., the change in momentum per unit time is equal to the net force, the change in pressure may be calculated as

$$\Delta P = -\rho L \frac{\Delta V}{\Delta t} \tag{1.1}$$

If the flow velocity at a point in the pipe changes suddenly from 1 m/s to zero due to the closing of a valve in one second, the change in the pressure is equal to (10^6) N/m^2 which is about a hundred plus/minus the initial pressure in the system. This explains why piping systems may fail when a transient event happen. Also, Newton's second

law can be used to derive Joukovsky formula to show that the change in pressure (Chaudhry, 2014). It may be expressed as

$$\Delta P = -\rho a \Delta V \tag{1.2}$$

where a is the wave velocity.

Another example mentioned by Karney (1990) to asses and visualize the magnitude of the energy transformation during a transient event in a piping system, supplies substantial physical insight: For $V = 2$ m/s with the same piping system parameters mentioned above, momentum of 2 (10^6) kg.m/s, and kinetic energy of 2 $(10^6)J$ are generated in the system. For the same previous valve scenario, the rate of transformed energy would be about 2 MW. This high rate of energy are common during transient events (Karney, 1990).

Researchers have been studying hydraulic transients for more than a century, and in the last few decades, significant advances have been made. Furthermore, modeling of transient conditions in closed conduits has considerably progressed especially during the era of powerful computers. The following paragraphs until the end of this section are based on material presented in Khilqa et al. (2019).

If the assumptions for the governing equations, i.e., the continuity and the momentum equations, are valid and the restrictions (e.g., stability and accuracy criteria) on the numerical procedures are satisfied, the computed results are reliable and may be used with confidence for design and operation of the systems. Most likely maximum and the minimum pressure peaks occur during the first cycle of the pressure head oscillations and usually, the first peak is used for design.

In the steady or quasi-steady friction approaches, the energy losses are attributable to wall friction. These losses are modeled using Darcy-Weisbach formula with a constant friction factor that can be determined from Reynolds number and relative roughness in Moody diagram for the initial steady flow state.

Piping systems are commonly designed to withstand the first transient pressure peak, which is unaffected by dissipation as discussed above. However, for multiple operations of control equipments, e.g., pump start-up following a power failure in a pumping system, load acceptance following load rejection on hydraulic turbines, etc., an accurate prediction of the dissipation of pressure oscillations is needed to determine a suitable time for the second operation. Therefore, including the dissipation in the simulation is very important. Transient conditions may become worse for multiple operations than that for a single operation.

Regardless of the significant advances in the modeling of transient flows in pressurized closed conduits in recent years as discussed above, the dissipation in computed transient oscillations with time is slower than that in real-life applications. In other words, the observed pressure head oscillations dampen faster than the computed results. The reason for the differences between the experimental data and computed results appears to be the use of steady-friction in simulations.

As discussed in detail in the next chapter, three different models or approaches have been used to simulate transient events for a sudden or gradual valve closure. However, the models have shortcomings in applicability, and thus they are not used extensively with confidence. Some of these models are computationally intensive and need huge memory. Others, depend on calibrated coefficients to model the dissipation accurately. The values of these coefficients vary over a wide range, and no formula or criteria is available to specify them for design. Also, to implement these models, a numerical solution of the governing equations (i.e., the continuity and momentum equations) for the entire piping system is required. Moreover, all available models provide a deterministic solution, i.e., a single value of pressure head oscillations at a specific time. It is a fact that all measurements or estimated values of different parameters have some uncertainty (Taylor, 1997). For example, the wave velocity may change 50% due to the amount of air in the system (Pearsall, 1965). In other

words, a universal computational procedure that is suitable for real-life applications by practitioners or precise estimation of parameters are not presently available.

Faced with a similar situation, structural engineers have been utilizing a simple technique for many years to handle the dissipation of vibrations of large structures, such as bridges, buildings, sports arenas, etc. Following this approach, a similar attempt is presented. In structural dynamics, damping is also a complex phenomenon similar to transient pressurized flows. For the dynamics of buildings and other complex structures, there is no specific methodology to simulate the damping for each structure. However, this complex problem is simplified by using a second-order linear ODE to track the displacements with an assumed damping ratio. In transient flow, using an ordinary differential equation to track the pressure oscillations is a satisfactory assumption (Jaeger, 1948). The author assumes that the damping and the pressure head oscillations are similar to those in structural dynamics. Even though damping is a complex problem, it may be simplified as a free vibrating spring. This simplification representing underdamped oscillations of lumped systems is adopted for simulating the pressure head oscillations in transient pressurized flows although this is a complex phenomenon, mechanics of which is not well-understood. Admittedly a gross simplification; but perhaps worth the effort for real-life applications until a more elegant procedure becomes available. The advantages of this simple model are: it is easy to apply, not necessary to analyze the entire system, it is not computationally intensive, and reasonable results suitable for practical applications are obtained. On the other hand, the limitations of the model are: it is used for a single pipe and it is an approximate method.

1.2 Objectives and scope of the dissertation

Based on the preceding discussion, a new model is needed to simulate a simple reservoir-pipe-valve system. The new model should be simple, reliable and practical

for real-life applications, and it should not be computationally intensive. Furthermore, the uncertainty should be quantified to apply the model with confidence.

The objective of the present work may be summarized as follows:

1. Develop a new model to simulate pressure head oscillations in closed conduits for a reservoir-pipe-valve system that is simple, and reliable for real-life applications.

2. Investigate the effect of different parameters on the damping of the pressure head oscillations.

3. Study the applicability of the model for the case of instantaneous or gradual valve closure.

4. Quantify the uncertainty of the model using Bayesian inference approach.

5. Determine the one-coefficient and two-coefficients values for 17 experiments.

6. Determine the damping percent due to using one- coefficient or two- coefficients models.

1.3 Structure of dissertation

In this dissertation, chapter 1 is an introduction to transient flows in pressurized closed conduits. Chapter 2 is an extensive literature review for the available models to simulate the pressure head oscillations in pressurized closed conduits. Chapter 3 represents a new model study to simulate the pressure head oscillations in pressurized closed conduit, followed by Chapter 4 to quantify the uncertainty for pressure head oscillations using Bayesian inference approach. Then Chapter 5 covers applications for Instantaneous-Acceleration-Based models. Finally, Chapter 6 presents the summaries and conclusions.

Chapter 2

Literature review

There are three main categories of models to simulate pressure head oscillations in piping systems: Steady one and two-dimensional models, Convolution integral (CB) models and Instantaneous Acceleration-based (IAB) models. These models are discussed in more details in the following sections.

2.1 Quasi one and two-dimensional models

The steady models, the friction force is calculated from the steady friction formula in solving the continuity and momentum equations that describe transient pressurized flows or so-called waterhammer phenomenon in closed conduits, i.e., these models assume that the wall-shear to averaged velocity in steady-state flows are valid at every instant during transient flow. In other words, steady model use the steady friction formula in solving classical waterhammer equations where the friction forces are simulated with a constant friction factor. In these models, Darcy-Weisbach equation is usually utilized to handle the friction losses. Usually steady-one-dimensional models are used to calculate the first and the second peaks of pressure head oscillations. The reason for the lack of agreement between the damping in computed and experimental or field data results appears to be mainly due to the use of steady friction formula to describe the dissipation (Ghidaoui et al., 2005). This modeling error in these models can be significant (Axworthy et al., 2000).

The two-dimensional models are computationally intensive, and assume that the flow has an axisymmetric profile and turbulence models are used to solve for the

velocity profile (Nixon and Ghidaoui, 2007). Since these models are computationally intensive, they have been used for simple piping system and simple boundary conditions (Reddy et al., 2011). Many researchers have reported these models such as (Vardy and Brown (2003), Vardy and Hwang (1991), Silva-Araya and Chaudhry (1997), Pezzinga (2000), and Zhao and Ghidaoui (2003)).

2.2 Convolution integral models

These are also called Convolution-Based (CB) methods or physically-based unsteady friction models. In addition to the steady friction resistant forces, these models use weighting functions and previous fluid local accelerations, named as unsteady friction, to include the resistant forces in solving the continuity and momentum equations of transient pressurized flows. In other words, the total instantaneous wall-shear stress consists of the quasi-steady friction as well as weighting function for the past acceleration. Therefore, they provide better simulation of damping as compared to that in the previous models. Unsteady friction, J_u, may be expressed mathematically using a weighting function, W, as

$$J_u = \frac{16\nu}{gD^2} \int_0^t \frac{\partial V}{\partial t}(t^*) W(t - t^*) dt^* \tag{2.1}$$

where ν = kinematic viscosity, D = pipe diameter, g = gravitational acceleration, V = flow velocity, and t = time, t^* = convolution time. Because these models account for the past velocity changes at every pipe section, many coefficients of the weighting function need to be stored in the memory of the computer. In addition, they are computationally intensive and time consuming and are mainly used for laboratory use.

These models become demanded especially with respect to the computer storage and performance (Storli and Nielsen, 2010). Many researchers have been interested in these model and have made significant contributions such as Zielke (1968), Trikha

(1975), Schohl (1993), Ghidaoui et al. (2002) and Vardy and Brown (2003, 2004) to increase their efficiency and accuracy. However; these are at the expense of computational speed (Vítkovskỳ et al., 2006).

2.3 Instantaneous Acceleration-based (IAB) Models

These are also called empirical-based models. The energy losses during the transient state in these models are considered as the sum of steady friction and unsteady friction due to instantaneous accelerations. The unsteady friction in these models caused by the temporal (local) acceleration and the convective (spatial) acceleration of the fluid. These models may be further divided into two categories: one-coefficient and the two-coefficient models. A model combining the effect of the temporal and the convective acceleration together is called one-coefficient model, while one considering the effect of the temporal and the convective accelerations separately is called two-coefficients model. These models do not consider the past acceleration step but rather on the instantaneous flow acceleration. Mathematically, the one-coefficient may be expressed as (Vítkovskỳ et al., 2006)

$$J_u = \frac{K}{g}\left[\frac{\partial V}{\partial t} + \text{Sign}\left(V\frac{\partial V}{\partial x}\right)a\frac{\partial V}{\partial x}\right] \tag{2.2}$$

where K = instantaneous flow acceleration damping coefficient, a = wave velocity, $Sign(V) = \pm 1$, and x = distance in x-direction along the pipe. A formula for the two-coefficients model may be written as

$$J_u = \frac{1}{g}\left[K_{ut}\frac{\partial V}{\partial t} + K_{ux}\,\text{Sign}\left(V\frac{\partial V}{\partial x}\right)a\frac{\partial V}{\partial x}\right] \tag{2.3}$$

K_{ut} and K_{ux} are coefficients for the temporal and convective accelerations, respectively.

Many researchers have developed these models such as, Daily et al. (1955), Brunone et al. (1991), Pezzinga and Scandura (1995), and Vítkovskỳ et al. (2006). These models are faster than CB models, and thus different boundaries can be easily analysed. In

addition, they are easy for numerical computations (Adamkowski and Lewandowski, 2006). On the other hand, the main shortcoming of these models is the selection of the values of K, K_{ut}, and K_{ux} which may vary over a wide range. Therefore, proper selection of these coefficients has been challenging due to the absence of any formula or criteria in this purpose. For examples, Reddy et al. (2011) report that K ranges from 0.015 to 0.060, K_{ut} varies between 0.006 to 0.057, and K_{ux} varies between 0.025 to 0.053, Bergant and Simpson (1994) report a range between 0.033 to 0.085 for K, Bughazem and Anderson (1996) report values between 0.065 to 0.15 for K. Vardy and Brown (1996) proposed theoretical values between 0.00827 to 0.138 for K. Moreover, these coefficients may change based on the method for solving the momentum and the continuity equations describing the transient pressurized flows.

2.4 Unsteady Friction

Since the 1950s, researchers have been developing models for hydraulic transient analyses, taking into consideration the losses due to unsteady friction. An outstanding paper on the review of the unsteady friction models by Ghidaoui et al. (2005). Summarized review contributions as follows:

1. Daily et al. (1955) are the pioneers for including the unsteadiness effects in computing the energy losses, by adding a term to account for the unsteady friction effect. They proposed an equation to compute J_u as

$$J_u = J_s + K\frac{D}{V^2}\frac{dV}{dt} \tag{2.4}$$

   where J_s is the steady friction factor. Daily et al. (1955) reported values for K between 0.2 to 1.2 for decelerating and accelerating turbulent flows, respectively.

2. Holmboe and Rouleau (1967) report the effect of viscous shear to be frequency-dependent and presented data for laminar and turbulent transient flows, which became a benchmark for later studies.

3. Zielke (1968) is the first researcher who provided an analytical solution for the transient pressurized laminar flow. Zielki applied Laplace transform and found that weighting functions act on the velocity profile under the assumption that unsteady laminar flows are stable. His solution was the foundation to develop models, called later as CB models.

4. Trikha (1975) simplified Zielki's solution by using an exponential relationship to approximate the solution in order to reduce the number of computations. His solution improves the computational speed; however, it is at the expense of accuracy (Vítkovskỳ et al., 2006).

5. Kita et al. (1980) proposed a variable eddy viscosity for Reynolds stress. They indicate that the predicted magnitude of the instantaneous friction factor is greater than that during the steady state for accelerating flows, while it is smaller, for decelerating flows.

6. Kagawa (1983) presented an efficient approximation method for simulating friction for transient laminar flow for Zielke's exact weighting function.

7. Suo and Wylie (1989) presented a numerical method for the impulse response to compute transients using frequency-dependent friction.

8. Brunone et al. (1991) postulated that the energy losses due to the unsteady friction are caused by the local and convective acceleration of the flow. Their model is referred to as IAB. They proposed a formula for the unsteady friction as

$$J_u = \frac{K}{g}\left(\frac{\partial V}{\partial t} - a\frac{\partial V}{\partial x}\right) \tag{2.5}$$

9. Eichinger and Lein (1992) presented a procedure to improve unsteady friction term by computing the velocity gradient in the radial direction for laminar and turbulent flows.

10. Vardy and Hwang (1991) verified the accuracy of Zielke model for one-dimensional expression for laminar flow. Vardy and Hwang (1993) extended the previous work to moderate turbulent flow. Then the work is extended further to include turbulent flow at high Reynolds number (Vardy and Brown, 1996). Overall, this work depends on the eddy viscosity region and how it can be split into two or five regions in order to simulate the Reynolds stresses.

11. Pezzinga and Scandura (1995) provided an analytical solution for frictionless pipelines with additional pipe of high-density polyethylene (HDPE) of unsteady flow oscillations. Besides, they found that using such viscoelastic pipe in a piping system reduces the unsteady flow oscillations.

12. Bughazem and Anderson (1996) studied the model presented by Brunone et al. (1991) and indicated the need for a simple unsteady friction model for complex piping systems.

13. Silva-Araya and Chaudhry (1997) developed a two-dimensional model to compute the unsteady friction losses in transient flow where the energy dissipation is estimated from the velocity profile. The model is applicable for both laminar and turbulent flows. A good agreement between the computed results and the experimental measurements was obtained, but required significant of computational effort.

14. Das and Arakeri (1998) observed forming a helical vortex which makes the velocity profiles during the transient event unstable with reverse flow near the wall of the pipe. They postulated that the unsteady boundary layer separation at high Reynolds numbers is due to instability of the reverse flow region.

15. Brunone et al. (2000) measured the velocity profile at different times during the transient state in a polyethylene pipe. They reported values of $K = 0.11$ and

0.25 for their experiments.

16. Pezzinga (2000) reported charts analogous to Moody diagram to aid in determining the value of the unsteady friction coefficient as a function of Reynolds number and relative roughness of the pipe. He applied dimensional analysis to determine the dimensionless parameters for unsteady friction.

17. Vítkovskỳ et al. (2000) investigated different numerical schemes. They presented a new model to overcome the shortcomings of the original Brunone et al. (1991) model with an updated formula for the unsteady friction as

$$J_u = \frac{K}{g}\left(\frac{\partial V}{\partial t} + \mathrm{Sign}(V)\, a \left|\frac{\partial V}{\partial x}\right|\right) \tag{2.6}$$

18. Bergant et al. (2001) investigated Zielke's model and verified it for low Reynolds number. Ramos et al. (2004) analyzed the unsteady friction in turbulent regimes and presented an approach based on the empirical corrective coefficients for local and convective acceleration in unsteady friction models.

19. Bughazem and Anderson (2000) investigated Brunone et al. (1991) model and demonstrated it can be used in practical waterhammer codes that gives good agreements with experimental results over a wide range of transient events.

20. Ghidaoui and Mansour (2002) derived an equation to approximate Vardy-Brown unsteady friction. This approximation is more efficient as compared to (CB) model from computational speed perspective.

21. Brunone et al. (2004) discussed unusual characteristics of transient laminar flow, and presented a good literature review prior to 2004. In addition, they pointed out that for viscoelastic pipes, K is only constant in turbulent transient flows.

22. Ramos et al. (2004) analyzed the unsteady friction in turbulent regimes and presented an approach based on the empirical corrective coefficients for local and convective acceleration in unsteady friction models.

23. Abreu and Almeida (2004) calculated wall shear stress from the cross-sectional distribution of axial velocities, and showed theoretically that unsteady contribution has two components: a dissipation component and a mostly dominant inertial component.

24. Adamkowski and Lewandowski (2006) presented a comparison between quasi-steady friction model and the following five different models: Zielke (1968), Trikha (1975), Vardy and Brown (2003), Zarzycki (1994), and Brunone et al. (1991).

25. Vítkovskỳ et al. (2006) tested unsteady friction models for eight different types of transient events by using convolution based (CB) and instantaneous acceleration based (IAB) models. They reported that the CB is valid for all events but IAB showed poor matches for the transients caused by instantaneous valve opening.

26. Nixon and Ghidaoui (2007) studied the unsteady friction in simple system with external fluxes due to demands, leaks, and other system elements. They showed that the unsteady friction effect may be neglected when the initial lateral flow is greater than 30% of the mean pipe flow. They concluded that the effect of unsteady friction is not critical for systems with large external flow.

27. Bergant et al. (2008a,b) develop a mathematical model and studied a number of cases to include the effects of different parameters that are not included in the classical waterhammer equations.

28. Pothof (2008) presented an idea for modeling under the CB models, and discussed different approaches of unsteady friction. He reported that unsteady friction is dominant during valve closure while steady friction models show reasonable damping for Reynolds number greater than 100,000.

29. Duan et al. (2010) presented an analysis for the visco-elastic pipes. They reported that the damping of pressure head oscillations is attributable to visco-elastic effects which becomes dominant in damping and phase shift at later stages, while the unsteady friction is relatively comparable with the visco-elastic effects during initial stages.

30. Vardy and Brown (2010) re-examined Zielke's model and presented a simple method to eliminate the error without using small grid for the integration time step.

31. Storli and Nielsen (2010, 2011) investigated Zielk's model and claimed that the reason of reporting a wide range of K belongs to changing local unsteady friction due changes in the pipe length. Also, they reported that both K_{ut} and K_{ux} vary with respect to space and time.

32. Reddy et al. (2011) developed an equation by using genetic algorithms to estimate unsteady friction coefficients for (IAB) models for instantaneous valve closure in elastic pipes.

33. Duan et al. (2012) investigated the importance of pipe system scale, the ratio of the pipe diameter to the length, on unsteady friction factor and found that the implication of the role of unsteady friction on the damping rate of the transient envelope diminishes with the pipe length and pipe diameter ratio.

34. Meniconi et al. (2014) presented a model that does not depend on the heuristic data and derived formulas to estimate the damping of the transient envelope by solving the governing one-dimensional transient flow equations in a dimensionless form; however, their formulas are limited to rapid valve closure cases. One of their formulas is for the case of the smooth pipe and another for the rough

pipe. Their formulas to compute total damping are somewhat complicated, thereby making it difficult for real-life applications.

35. Martins et al. (2016) used computational fluid dynamic model to investigate transient energy dissipation. They reported that CB models describe the pressure signals better than IAB models due to the past time step.

36. Duan et al. (2017) investigated the importance of the unsteady friction for different models. They concluded that the use of unsteady friction or turbulence models is necessary for transient flow simulation in small scale pipe systems with high frequency behavior. They reported that the IAB model are more accurate than CB models to simulate the maximum and minimum envelopes. However, for designing piping system, the CB model are more reliable.

Chapter 3

Damping in Transient Pressurized Flows *

3.1 Introduction

Significant advances have been made during recent years in the modeling of transient flows in pressurized closed conduits initiated by changes in the settings of the flow controls equipment. If the assumptions that form the basis of the governing equations are satisfied and the stability and accuracy criteria for the numerical procedures are observed, the computed results are reliable and may be used with confidence for system design and operation. However, the dissipation of the transient oscillations with time is not completely understood at present, and the dissipation in the computed results is usually slower than that in the real-life systems. Mostly, this difference between the computed and measured results is attributed to the use of steady-state friction equation to compute energy losses during the transient state in which the damping is calculated using the steady friction formula while solving the continuity and momentum equations that describe transient-flows phenomenon in closed conduits.

The first peak in transient state pressures is usually not affected by the dissipation of pressure oscillations. The dissipation of pressure oscillations is not considered very important in most cases and this peak pressure is typically utilized for design and operations. However, for multiple control operations in a system, such as starting

*Khilqa, S., M. Elkholy, M. Al-Tofan, J. M. Caicedo, and M. H. Chaudhry (2019). Damping in transient pressurized flows. *Journal of Hydraulic Engineering,* http://doi.org/10.1061/(ASCE)HY.1943-7900.0001624. Reprinted here with permission from ASCE

the pumps following power failure or pump shutdown, opening or closing of control valves following the closing or opening operations in piping system, or load acceptance following load rejection on turbines in a hydro-power plant, it is very important to determine the dissipation of the pressure oscillations so that the second operation is started in time to reduce the severity of the subsequent transient conditions. If this is not done properly, the resulting transient conditions may be worse than that for a single operation. Therefore, knowing the magnitude of the dissipated pressure oscillations at different times after the first or the second peak is important in multiple operations (Chaudhry, 2014).

The inclusion of energy losses in the computations of transient flows has been investigated for many decades worldwide and several computational procedures have been reported. However, in the authors' opinion, a universal computational procedure that is suitable for real-life applications by practitioners is not presently available. This is because transient flows are very complex and extremely rapid. In addition, instrumentation for the precise measurement of various variables of interest or for the visualization of flow for understanding the mechanics of various process are not available. For similar situations to predict the dissipation of vibrations of large structures, such as bridges, buildings, sports arenas, etc., structural engineers have been utilizing a simple technique for many years. Following this approach, a similar method is presented in this paper to handle the complex phenomenon of dissipation in transient flows, the mechanics of which are not well-understood at present. A simple equation describing under-damped oscillations of lumped systems is utilized for this purpose. This is admittedly a gross simplification; but perhaps worth the effort and suitable for consideration for real-life applications until a more elegant procedure becomes available.

Three classes of methods used to simulate the dissipation of transient pressures are: two-dimensional models, the convolution integral methods and the instantaneous

acceleration-based methods. All of these methods require the simulation of transients in the entire system. The first two are computationally intensive and the selection of the suitable coefficients for the third is somewhat difficult and challenging. As a result, these methods have not been adopted for general, real-life applications (Reddy et al. (2011), Adamkowski and Lewandowski (2006), Zhao and Ghidaoui (2004) and Ghidaoui et al. (2005)). Although some of these models give satisfactory results for the damping of pressure oscillations in a simple piping system, they may not be reliable and applicable in complex cases. Quasi two-dimensional models and convolution based integral models are computationally intensive (Chaudhry, 2014; Weinerowska-Bords, 2015). Nowadays, most researchers are using instantaneous-acceleration-based (IAB) models. These models may be classified further as one-coefficient or two-coefficient models. Proper selection of the coefficients for the one- or two-coefficient models has been challenging. The coefficients vary over a wide range. In addition, the implementation of these models requires the simulation of the entire system.

Pezzinga and Scandura (1995) presented an analytical solution for frictionless pipelines and for high-density polyethylene (HDPE) pipe, by considering both as elastic. Bughazem and Anderson (1996) studied the model presented by Brunone et al. (1991) and indicated the need for a simple, unsteady friction model for complex piping systems. Pezzinga (2000) prepared charts similar to Moody diagram to select the unsteady coefficient depending on the Reynolds number and the relative roughness of the pipe and applied dimensional analysis to determine the dimensionless parameters for unsteady friction. Bergant et al. (2001) investigated Zielke's model and verified it for low Reynolds numbers. Ramos et al. (2004) analyzed the unsteady friction in turbulent flows and presented an approach based on the empirical corrective coefficients for local and convective acceleration in unsteady friction models. Adamkowski and Lewandowski (2006) presented a comparison between quasi-steady friction model and the following five different models: Zielke (1968), Trikha (1975),

Vardy and Brown (2003), Zarzycki (1994), and Brunone et al. (1991) models.

Recently Meniconi et al. (2014) presented a model that does not require the heuristic data and derived formulas to estimate the damping of the transient envelope; it instead solves the governing one-dimensional transient flow equations in a dimensionless form; however, Meniconi et al.'s formulas are limited to instantaneous valve closure. One of their formulas is for a smooth pipe and another for a rough pipe. Their formulas to compute total damping are somewhat difficult for real-life applications.

The objective of the present work is to present a simple, reliable model that is not computationally intensive and can predict the dissipation of the pressure head oscillations. For illustration purposes, the model is applied to a simple reservoir-pipeline-valve system for instantaneous and gradual valve closure. In this paper, a dissipation method is developed following a method used for computing the dissipation of structural vibrations. Subsequently, an expression for the damping ratio is developed using dimensional analysis and by non-linear regression. The computed results are compared with the experimental measurements and discussed in detail, then the uncertainty quantification is discussed, followed by a summary and conclusions.

3.2 Under-damped System

The closure of a downstream valve in a reservoir-pipeline-valve system results in pressure head oscillations at the valve that are similar to the oscillations of the mass in a spring-mass-damper system (Fig. 3.1). The displacement of the oscillating mass exhibits an exponential decay due to viscous damping which may be studied as free vibrations, i.e., no external force. For example, damping in a single degree of freedom of a structure may be simulated as a linear viscous damper (Chopra et al., 2012).

The following governing equation describes the displacement, x, of mass, m (Fig. 3.1) with respect to time, t.

$$m\ \ddot{x}(t) + c\ \dot{x}(t) + k\ x(t) = 0 \tag{3.1}$$

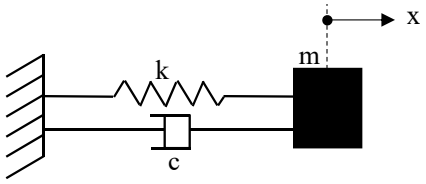

Figure 3.1: Spring-mass system

This is a second-order ordinary differential equation in which c = damping constant as a measure of the energy dissipation and k = spring constant. Equation 3.1 may be rewritten in its auxiliary form (Kreyszig, 2010) as

$$m\ r^2 + c\ r + k = 0 \tag{3.2}$$

The roots of this equation are

$$r_1 = \frac{-c + \sqrt{c^2 - 4\ m\ k}}{2m} \tag{3.3a}$$

$$r_2 = \frac{-c - \sqrt{c^2 - 4\ m\ k}}{2m} \tag{3.3b}$$

The following three cases of damping are possible depending on the value of $(c^2 - 4mk)$: *overdamped* if $c^2 - 4mk > 0$; *critical damping* if $c^2 - 4mk = 0$; and *underdamped* if $c^2 - 4mk < 0$. The dissipation of pressure head oscillations at a section in a piping system are similar to that in the underdamped case (Similarities and differences between a vibrating spring-mass and hydraulic systems are explained in Chaudhry (2014)) as follows. The damping of the pressure head oscillations is similar to those in structural dynamics where displacement is described as a free vibrating spring-mass. Even though in structural (building) dynamic the damping is a complicated problem, it is simplified as a free vibrating spring-mass problem. The authors follow this simplification for simulating the pressure head oscillations in transient pressurized flows. The current study focuses on formulating a model to determine the damping ratio, ζ, of the pressure heads oscillations in a reservoir-pipe system due to closure of the

downstream valve, assuming that a lumped system describes the pressure variation in the time domain.

The pressure head deviation, $h = H - H_s$, may be written as

$$m\frac{d^2h}{dt^2} + c\ \frac{dh}{dt} + k\ h = 0 \tag{3.4}$$

where H is the pressure head at the downstream valve and H_s is the head at the upstream reservoir (static head). Equation 3.4 is a linear, second-order ordinary differential equation. Although equations that describe the transient flow are nonlinear, this linear approximation is acceptable as long as the goal is to estimate the damping of the transient envelope. In addition, this approximation is considered satisfactory in practice (Jaeger, 1948). The general solution of Eq. 3.4 for the underdamped case is

$$h(t) = e^{-\left(c/2m\right)t}\left(c_1 \cos\left(\omega t\right) + c_2\ \sin\left(\omega t\right)\right) \tag{3.5}$$

This solution has the same form as the analytical solution developed by Duan et al. (2012) to investigate the unsteady friction damping of transient pressures in one-dimensional flow. They linearized the non-linear quasi-friction term and found that the pressure head in the frequency domain, $H^*(x^*, \omega^*)$, may be written as

$$\frac{\partial^2 H^*}{\partial x^{*2}} + C_L\ H^* = 0 \tag{3.6}$$

where $x^* = x/L$ is the relative distance with L as the length of the pipe; ω^* is the frequency of the pressure head oscillations and C_L is a lumped parameter for wave propagation. The solution of this equation has the following form

$$H^*(x^*, \omega^*) = H_o^*\ e^{(K_a + iK_p)x^*\omega^*} \tag{3.7}$$

where K_a and K_p are factors of wave attenuation and phase shift, respectively and $H_o^*, H/H_o$, is the relative pressure head oscillation, and H_o is the steady state head.

The last equation is similar to Eq. 3.5, which means that the current approach may be utilized for the pressure head oscillations.

Equation 3.5 may be further simplified as

$$h(t) = Ae^{-\left(c/2m\right)t} \sin\left(\omega t + \phi\right) \tag{3.8}$$

in which A is the amplitude of the pressure head at $t = 0$, ω is the frequency of the pressure oscillations, and ϕ is the phase shift of the wave. For the pressure head at the downstream valve, the phase shift may be assumed as zero. Hence, Eq. 3.8 becomes

$$h(t) = Ae^{-\left(c/2m\right)t} \sin\left(\omega t\right) \tag{3.9}$$

The sinusoidal wave solution for Eq. 3.4 is an odd function and a square wave can be replaced by a sum of the odd integer harmonics using Fourier series as:

$$h(t) = Ae^{-\left(c/2m\right)t}\Big(\sin\left(\omega t\right) + \frac{1}{3}\ sin(3\omega t) + \frac{1}{5}\sin\left(5\omega t\right) + \frac{1}{7}\sin\left(7\omega t\right) + ...\Big) \tag{3.10}$$

The exponent $(c/2m)$ is an unknown quantity with the dimension of (1/s) and it represents the rate of decay of pressure oscillations. This term equals to $(\zeta\ \omega_n)$ (Chopra et al., 2012) where ω_n is the natural frequency of the pressure oscillations at the valve . For simplicity, the fundamental harmonic is used in this paper. Equation 3.10 may then be written as

$$h(t) = Ae^{-\zeta\omega_n t} \sin\left(\omega_d t\right) \tag{3.11}$$

where ω_d is the frequency of pressure oscillations if damping is included and is called damped frequency, $\omega_d = \omega_n\sqrt{1-\zeta^2}$. Since ζ is small, ω_d may be assumed equal to ω_n (Humar, 2012). For an instantaneous valve closure at $t = 0$, A, may be determined from the Joukowsky formula; for gradual valve closure, a procedure to compute A is presented later.

For instantaneous valve closure, $\Delta h = \pm a\Delta V/g$ in which Δh is the increase in pressure head at $t = 0$, a is the wave speed, ΔV is instantaneous variation of the flow velocity at the valve, and g is the gravitational acceleration. In this, $A \cong \Delta h$. This value of A is an approximation for sinusoidal oscillations since the instantaneous closure results in square waves. The term $e^{-\zeta\omega_n t}$ represents damping of the oscillations, and the head deviation at the valve, h, approaches zero as t tends to infinity. In other words, Eq. 3.11 is an exponential decay function with ζ as the damping ratio, which is a function of the system parameters and boundaries, flow rate, and fluid properties. This equation may be used to compute the dissipation of pressure oscillations. The advantages of this model are: it is easy to apply, the entire system is not analyzed, it is not computationally intensive, and reasonable results suitable for practical applications are obtained. On the other hand, the limitation of the model is an approximate method that is applicable to a single pipeline.

3.3 Experimental Data

Two data sets are used in this paper: The first data set is obtained from the experiments conducted in the Hydraulic Laboratory at the University of South Carolina (USC), and the second set is from experiments reported in the literature. The USC experimental setup consists of a pressurized tank at the upstream end, a 158.71 m long copper pipe, 0.0254 m in diameter with 0.001 m wall thickness and a ball valve at the downstream end of the pipe, as shown in Fig. 3.2. To generate a transient condition, the ball valve at the downstream end is closed by a spring, triggered by a magnetic switch which allows for the closure of the valve in approximately 0.026 seconds. The pressure in the pipe is measured by a TJE pressure transducer, mounted on the pipe, just upstream of the valve. The pressure transducer is manufactured by Honeywell International Incorporation and has a pressure rating (design pressure) of 140 m with an accuracy of 0.1%. An electronic sensor is installed on the valve to

measure the variation of the valve angle with time during the closure. The pressure transducers and the electronic sensor are all wired to a data-acquisition board that has three digital hardware timers and triggers, assuring accurate timing for the valve closure and signal acquisition. The experiment is run until the flow in the pipe becomes steady. The magnetic switch is then triggered, creating a rapid valve closure and generating a transient state. A total of seven experiments are carried out. In this data set, Reynolds number ranges from 4,348 to 7,845. Table 3.1 lists the system data for these experiments. The second set of data is from experiments conducted in various laboratories all over the world. This data set covers a wide range of Reynolds number, ranging from 5,731 to 239,957, Mach number, and D/L. Table 3.2 lists the system data for these experiments.

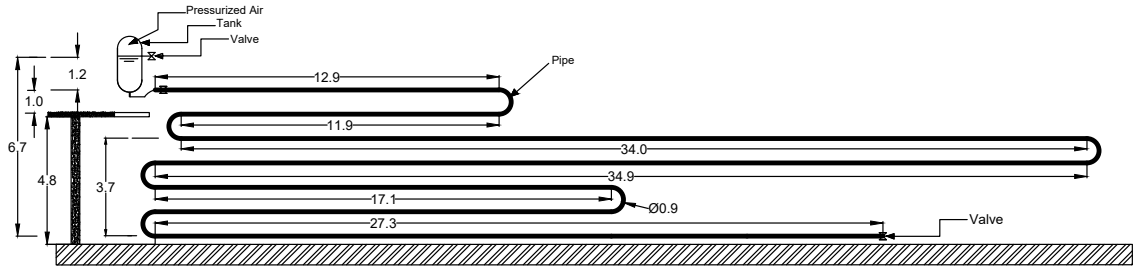

Figure 3.2: USC experimental setup. (All dimensions are in m)

Table 3.1: System data for present experiments

Test No.	H_s (m)	V_o (m/s)	Re_0 (V_oD/ν)	a (m/s)	Ma $\times 10^{-4}$ (V_o/a)	P
1	34.36	0.309	7845	1194	2.58	6.83
2	33.59	0.255	6482	1216	2.10	8.15
3	30.34	0.310	7876	1215	2.55	6.90
4	16.08	0.171	4348	1147	1.49	10.86
5	17.54	0.220	5597	1154	1.91	8.83
6	21.10	0.213	5410	1181	1.81	9.21
7	12.68	0.194	4918	1109	1.75	9.40

Table 3.2: System data for experiments reported in literature

Test No.	L (m)	D (m)	H_s (m)	V_o (m/s)	Re_0 (V_oD/ν)	a_{reported} (m/s)	ω (1/s)	a_{comp} (m/s)	Ma $\times 10^{-4}$	P
8^a	98.11	0.016	127.5	0.34	5731	1298	20.329	1270	2.68	6.42
9^a	98.11	0.016	127.5	0.631	10635	1298	19.894	1243	5.08	3.65
10^b	62.50	0.0127	61.0	0.485	5750	1250^*	30.241	1203	4.03	10.57
11^c	143.7	0.0532	24.8	0.18	8398	1360	14.504	1327	1.36	29.18
12^c	77.80	0.0532	25.0	0.18	8398	1363	26.745	1325	1.36	53.81
13^d	38.08	0.0254	10.0	0.240	7207	1350	58.758	1350	1.81	42.25
14^e	60.00	0.10	102.0	0.31	31000	1248.4	30.308	1158	2.68	82.08
15^f	4170	0.26	260	0.375	97584	1210	0.451	1198	3.13	2.07
16^f	4170	0.26	260	0.524	136139	1210	0.451	1198	4.37	1.48
17^f	4170	0.26	260	0.923	239957	1210	0.449	1191	7.75	0.84

Superscripts: a = Adamkowski and Lewandowski (2006); b = Bughazem and Anderson (1996);
c = Pezzinga and Scandura (1995); d = Holmboe and Rouleau (1967);
e = Carlsson (2016); f = Meniconi et al. (2014);
* = (1250 ± 40);
Pipe wall material: Tests No. 8, 9, 10 and 13 are copper; Tests No. 11 and 12 are zinc-plated steel;
Tests No. 14, 15, 16 and 17 are steel.

3.4 Damping Ratio

Assuming the damping ratio is a function of the system characteristics

$$\zeta = \psi\left(L, D, V_o, \mu, \rho, K, E, e, \epsilon, g\right) \tag{3.12}$$

where L is the length and D is the diameter of the pipe; V_o is the initial steady state flow velocity; μ is the dynamic viscosity of the fluid; ρ is the fluid density; ϵ is the absolute roughness of the pipe; K is the bulk modulus of elasticity of the fluid; E is Young modulus of elasticity; and e is the pipe thickness. A relationship by using dimensional analysis for the damping ratio may be written as

$$\zeta = \psi\left(\mathrm{Re}_0, \mathrm{Ma}, \frac{\epsilon}{D}, \frac{D}{L}, \frac{{V_o}^2}{Dg}\right) \tag{3.13}$$

where Re_0 is the Reynolds number; Ma is the Mach number $= V_o/a$; ϵ/D is relative roughness of the pipe ($\frac{{V_o}^2}{Dg}$) represents Froude number squared. The effect of Froude number is insignificant in transient pressurized flow, and is dropped. In the dimen-

sional analysis, K, E, and e represent the wave speed, which appears in the Mach number. Therefore, it is appropriate to consider them in terms of wave velocity in Ma in Eq. 3.13. The pipe inertia and axial pipe motion are not considered, which is acceptable for properly anchored piping systems (Tijsseling, 1996). The relative roughness is dropped for the following reasons: 1) In most of the tests done, the flows are hydraulically smooth; 2) Since the relative roughness is based on the pipe material, age, use and other factors, its value is not precisely known for inclusion it in the analysis; 3) Even if the relative roughness is taken into consideration, the exponent of its term is small (i.e., approximately 0.001) and can thus be practically neglected; 4) The change in the velocity profiles is the main factor for the damping in transient flows (Discussion of Plant et al. (1963) (typically flows near the wall and in the core move in opposite directions and vortices form at the separation zones). In addition, this is confirmed by numerical modeling by several authors (Brunone et al., 1991, 2000; Silva-Araya and Chaudhry, 1997; Vítkovskỳ et al., 2006).

Thus, Eq. 3.13 may be rewritten as

$$\zeta = (\mathrm{Re}_0)^{\theta_1} (\mathrm{Ma})^{\theta_2} \left(\frac{D}{L}\right)^{\theta_3} \tag{3.14}$$

where, θ_1, θ_2, and θ_3 are parameters.

For the damping ratio, a best fit technique is used to determine the corresponding value of the damping ratio for each experiment listed in Tables 3.1 and 3.2. Maximum value of the correlation coefficient, R^2, between the experimental data and the simulated results using Eq. 3.11 is used for the best fit. The damping ratio for the experimental measurements is obtained by using the best fit, and it is called, ζ_{bf}.

Using non-linear regression analysis for the experimental data for 17 experiments and corresponding, ζ_{bf}, a relationship is developed for the damping ratio, ζ, as a function of the non-dimensional groups of Eq. 3.14 as

$$\zeta = {\mathrm{Re}_0}^{0.04}\ {\mathrm{Ma}}^{0.632} \left(\frac{D}{L}\right)^{-0.062} \tag{3.15}$$

The correlation coefficient, R^2, between ζ_{bf} and ζ of Eq. 3.15 is 0.83. Figure 3.3 shows a comparison between ζ_{bf} that is obtained from the best fit technique for the experiments, and ζ computed from Eq. 3.15. The range of Re_0, Ma, and D/L used in this analysis are (4.35×10^3 to 2.40×10^5), (1.36×10^{-4} to 7.81×10^{-4}), and (6.24×10^{-5} to 1.67×10^{-3}), respectively. It is worth mentioning that the data used in deriving Eq. 3.15 is for elastic pipe materials and the flow is turbulent.

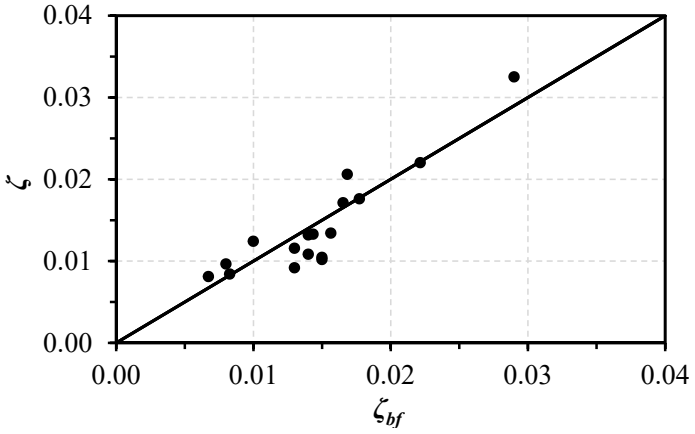

Figure 3.3: Comparison between the best fit and computed damping ratio

3.5 Gradual Valve Closure

In real-life applications, valves are opened or closed gradually to minimize transient pressures. However, Eq. 3.11 cannot be used directly because Joukowsky formula is not applicable and thus the value of A cannot be computed from this equation. For gradual valve closure, the value of A may be determined from Eq. 3.11 as follows:

$$\frac{dh}{dt} = A\left[\omega e^{-\zeta\omega t}\cos\omega t - \zeta\omega e^{-\zeta\omega t}\sin\omega t\right] \tag{3.16}$$

The slope of pressure heads oscillations, (dh/dt), may be computed at the start of the first cycle of pressure oscillations i.e., $t = 0$, as shown in Fig. 3.4. Note that this time is not the same as that for the start for transients following instantaneous valve closure. By substituting $t = 0$, Eq. 3.16 becomes

$$\left(\frac{dh}{dt}\right)_{t=0} = A\omega \tag{3.17}$$

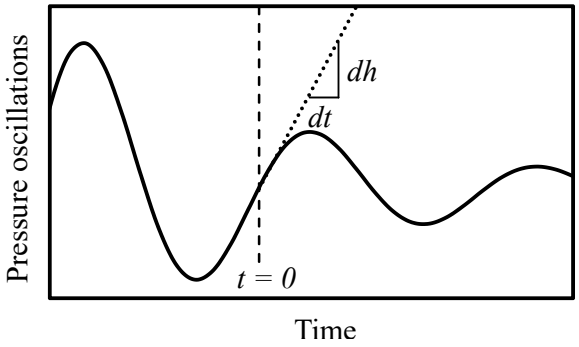

Figure 3.4: Slope $\left(\frac{dh}{dt}\right)_{t=0}$ in Eq. 3.17

Method of characteristics is used in the quasi-steady model to simulate the pressure head oscillations at the start of the first cycle, i.e., at $t = 0$. These computed results are used to determine the slope (dh/dt) by calculating it from two successive points. As stated earlier, steady friction formula is used in the quasi-steady model. To find the slope from experimental data, it is smoothed first. The smoother the data, the more accurate are the results. Moreover, it is intuitive that the slope is maximum or minimum when $t = 0$. For downstream valve closure, maximum slope is used to find the value of A, and for upstream valve closure, minimum slope is used to find the value of A.

To obtain data for verification, a number of experiments are conducted in USC Hydraulic Laboratory on the setup described previously. The valve is connected to a DC stepper motor which is controlled by a programmed code using LabVIEW (Kalkman, 1995) to allow for gradual valve closure (GVC). Three experiments are carried out along with an additional experiment from the literature. Table 3.3 lists the system data for these experiments and Fig. 3.5 shows the pressure oscillations for these experiments. In this table, T_c is the valve closure time.

Table 3.3: System data for gradual valve closure experiments

Test No.	H_s (m)	Re_0	Ma	D/L	T_c (s)	Reference
1	6.80	24183	0.00114	0.00016	3.5	present study
2	6.80	24183	0.00115	0.00016	10	present study
3	6.80	24183	0.00115	0.00016	18	present study
4	2.65	196106	0.00201	0.00316	1.085	Silva-Araya (1993)

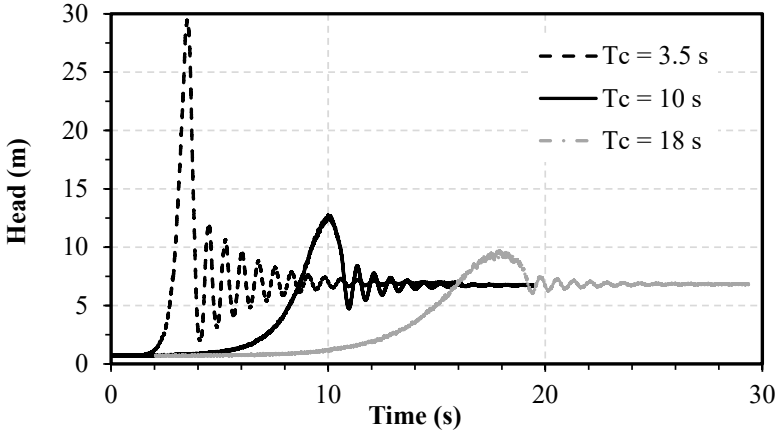

Figure 3.5: Pressure oscillations following gradual valve closure

3.6 Discussion

The effect of non-dimensional parameters, Re_0, Ma, and D/L on the damping ratio is investigated individually. Figure 3.6 shows the relationship between ζ_{bf} and Re_0. This figure shows that the damping ratio increases with increase in Reynolds number. However, the rate of increase is small for the low Re_0 turbulent region, but it has a steep gradient for $\mathrm{Re}_0 > 40{,}000$. The experimental damping ratio varies from 0.007 to 0.017 for $\mathrm{Re}_0 < 40{,}000$ and from 0.018 to 0.029 for higher Re_0. The sudden increase in the damping ratio for $\mathrm{Re}_0 > 40{,}000$ may be due to the formation of helical vortices that make the flow unstable (Das and Arakeri, 1998). Since flow instability alters the flow structure and the strength of the turbulence during transient flow (Ghidaoui and Kolyshkin, 2001), the rate of damping may increase considerably.

To investigate the behavior of damping ratio, a parameter, P, representing the ratio between the diffusion timescale and the waterhammer timescale is calculated.

This dimensionless parameter proposed by Ghidaoui et al. (2002), is expressed mathematically as $P = 2D/\left(\sqrt{f}\ L\ \mathrm{Ma}\right)$, where f is the steady state Darcy Weisbach friction factor. P measures the acceptability of the quasi-steady assumption in the modeling of transient flows. This shows that the quasi-steady assumption is acceptable for $P \gg 1$, and this assumption is questionable when P is of the order of 1. The variation of damping ratio, ζ_{bf}, with P is shown in Fig. 3.7. In this figure, for P ranging from 0.8 to 10, the change of the damping ratio is significant. Following earlier investigations, this may be due to the vorticity generated by the wave and to the mixing of the turbulence structure by the subsequent pressure waves (Pothof, 2008). It diffuses all the way to the pipe core and changes the pre-existing turbulent state (Duan et al., 2010). Figure 3.7 and Tables 3.1 and 3.2, indicate that the damping ratio in real-life systems is high with P approximately 4. However, for laboratory systems, the damping ratio is low and for corresponding P is much higher. This confirms findings by Ghidaoui et al. (2002) and Pothof (2008) that for $0.1 < P < 10$ the quasi-steady assumption is questionable.

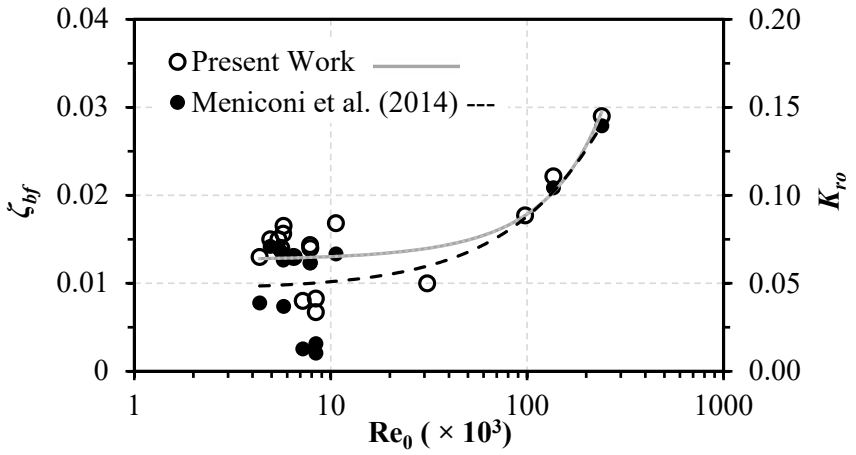

Figure 3.6: Damping ratio, ζ_{bf}, (present study) and K_{ro} (Meniconi et al. (2014)) as function of Re_0

As mentioned in the introduction, Meniconi et al. (2014) derived an analytical formula to calculate the total damping factor, K_{ro}, due to steady and unsteady friction

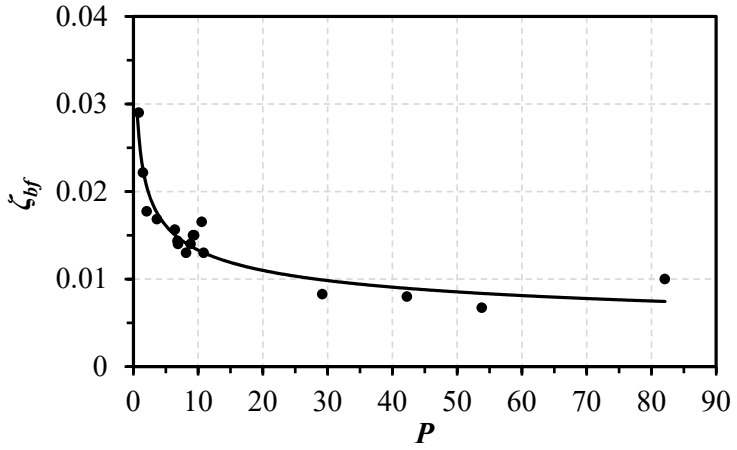

Figure 3.7: Damping ratio, ζ_{bf} vs. P

effects for smooth and rough flow pipes as

Smooth pipe:

$$K_{ro} = \begin{cases} \frac{f\mathrm{Re}_0}{2}\frac{T_w}{T_{dv}} + \sqrt{2\frac{T_w}{T_{dv}}}, & \text{if } \mathrm{Re}_0\frac{T_w}{T_{dv}} \ll 1 \\ \frac{f\mathrm{Re}_0}{2}\frac{T_w}{T_{dv}} + \frac{1}{30.33\mathrm{Re}_0{}^{0.94}}\frac{T_{dv}}{T_w}, & \text{otherwise} \end{cases} \tag{3.18}$$

Rough pipe:

$$K_{ro} = \frac{f\mathrm{Re}_0}{2}\frac{T_w}{T_{dv}} + 0.024\left(\frac{\epsilon}{D}\right)^{0.016}\left(Re_0\frac{T_w}{T_{dv}}\right)^{-0.414} \tag{3.19}$$

where, Re_0 is the initial Reynolds number, $T_w = L/a$ is the wave timescale, and $T_{dv} = D^2/\nu$ is the radial diffusion timescale, and ν is the kinematic viscosity. Their equations recommended the use of the instantaneous Reynolds number rather than the initial one since turbulent conditions during transients keep on changing. However, comparing the above equations using the initial Reynolds number shows good agreement with the damping factor, ζ estimated from Eq. 3.15. The ratio, $K_{r0}/\zeta = 4.2 \pm 1.8$ is estimated and the deviation here may be attributed to many other factors besides including the necessity of using instantaneous Reynolds number rather than the initial one. This comparison is shown in Fig. 3.6.

Figure 3.8 shows that ζ_{bf} increases with the increase in Ma. From the figure, it may be concluded that reducing the wave speed or increasing the Mach number

increases the damping ratio significantly.

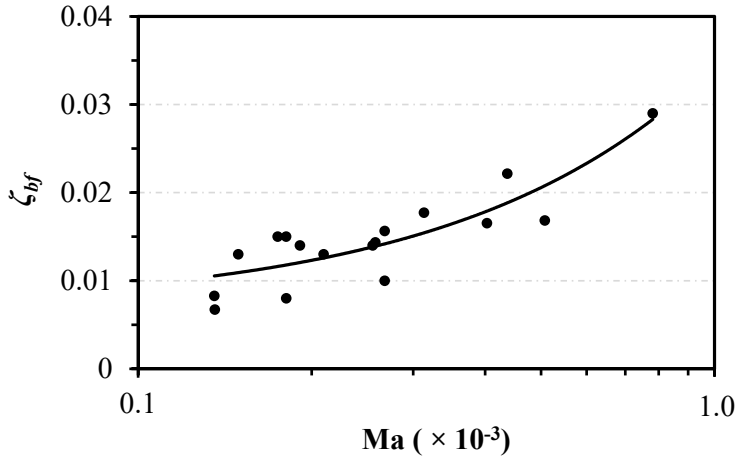

Figure 3.8: Damping ratio, ζ_{bf} vs. Ma

The variation of damping ratio, ζ_{bf}, with D/L is shown in Fig. 3.9. It shows that the ζ_{bf} decreases as D/L increases. For small ratio of D/L, ζ_{bf} has relatively high value and vice versa. The laboratory systems for D/L is greater than that for real-life systems due to the length of the pipe, because pipe length in laboratory is shorter as compared to the pipe length in the field.

Friction effects influencing the damping ratio may be divided into two parts: The first part is the damping due to steady friction, and due to unsteady friction. The length of the pipe plays an important role due to not only its effect on D/L ratio but also due to its effect on the frequency where it is inversely proportional to the frequency of the pressure head oscillations (frequency of the waterhammer wave). For a long pipe (i.e., real-life systems), the product of ω and ζ_{bf} is small (i.e., < 0.1). In contrast, for a relatively short pipe (i.e., laboratory systems), the product of ω and ζ_{bf} is large, and thus, another source for damping may be necessary. For example, the product $\omega \times \zeta_{bf}$ for tests No. 15 and No. 17 is 0.017 and 0.013, respectively, while it is 0.17 and 0.50 for tests No. 1 and No. 10, respectively.

In Table 3.2, the wave speeds, a_{reported}, are listed in relevant reference. For this study, wave speed, a_{comp}, is computed from the experimental pressure oscillations by

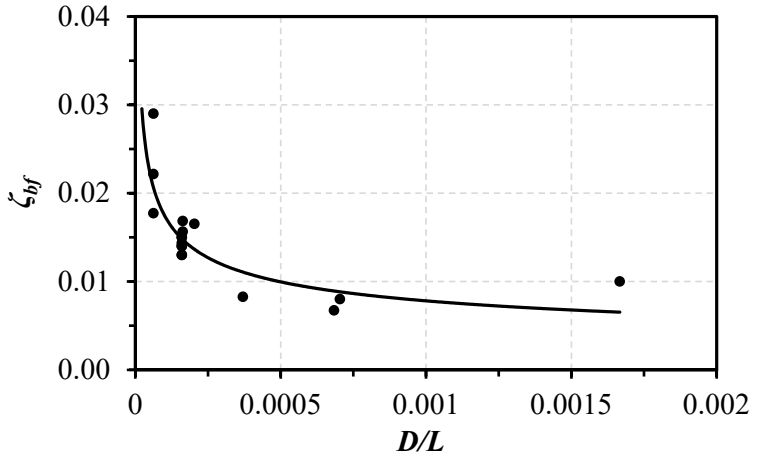

Figure 3.9: Damping ratio, ζ_{bf} vs. D/L

averaging wave speed for different cycles.

Figure 3.10 shows the comparison of the pressure head variations at the downstream valve for several tests between the experimental measurements and the results computed from Eq. 3.11 using ζ computed from Eq. 3.15. This figure shows that the simulation is in good agreement with the experimental measurements. However, some of the experimental and the computed values differ due to the use of the best-fit technique for calculating the damping ratio and the uncertainty in the nonlinear regression.

Figure. 3.11 compares the sinusoidal part of the pressure oscillations and corresponding experimental results for the gradual valve closure experiments. The slope is calculated by using quasi-steady model, A from Eq. 3.17, and ζ from Eq. 3.15. Then Eq. 3.11 is used to determine the pressure head oscillations. The comparison shows a good agreement between the experimental and computed results. Therefore, this method may be used to predict the pressure oscillations for gradual valve closure since the damping ratio is not a function of valve closure time. However, some discrepancies are noted between the experimental and computed results. This may be due to the calculation of the amplitude, A, which depends on the slope computed numerically. The slope of the pressure head oscillation is steeper for experiments

with short wave timescale, L/a, than those with long wave timescale, as shown in Fig. 3.11(d), where the length of the pipe is relatively short.

Additional experimental results for systems with different boundary conditions or for series systems are needed to verify the applicability of the developed relationship for the damping ratio.

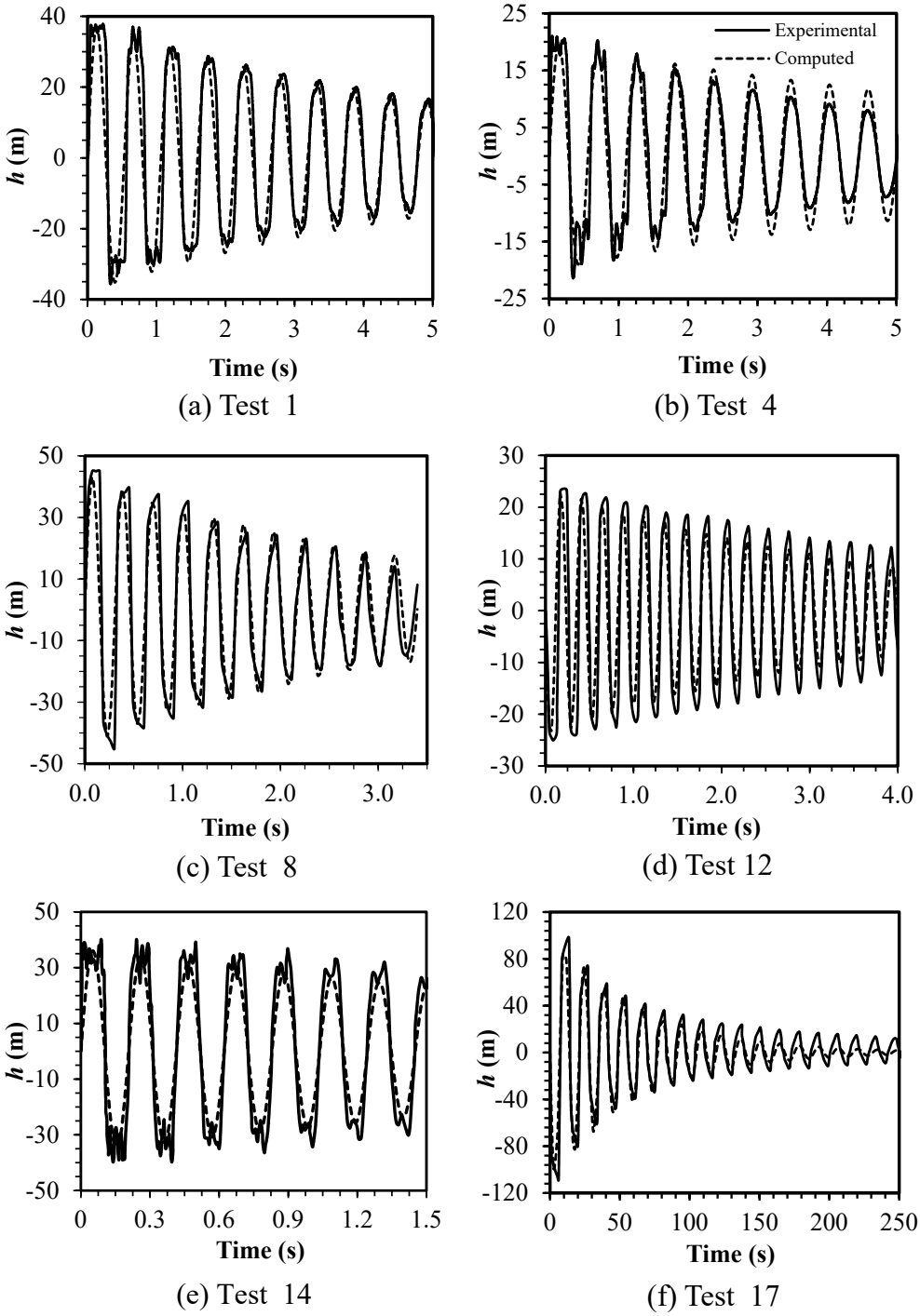

Figure 3.10: Comparison of experimental and computed pressure at the downstream valve

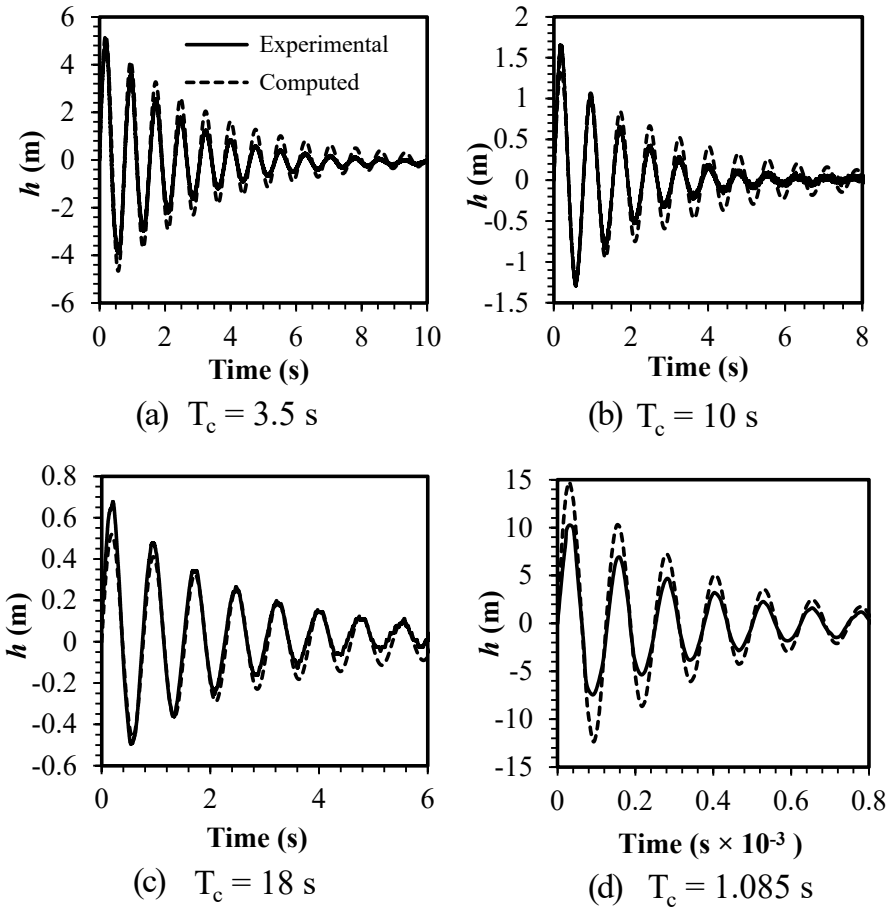

Figure 3.11: Comparison of experimental and computed pressure at gradually closing downstream valve

Chapter 4

Uncertainty Quantification for Damping in Transient Pressure Oscillations*

4.1 Introduction

In Chapter 3, a model for computing the damping of pressure head oscillations following instantaneous valve closure in a simple piping system is presented. The model is developed by using dimensional analysis and verified by comparing the computed results with experimental measurements using the equation

$$\zeta(\Theta, \mathrm{Re}_0, \mathrm{Ma}, D/L) = (\mathrm{Re}_0)^{\theta_1} (\mathrm{Ma})^{\theta_2} \left(\frac{D}{L}\right)^{\theta_3} \tag{4.1}$$

where Re_0 is the Reynolds number, Ma is the Mach number, D/L is the ratio of diameter to length of the pipe, and $\Theta = \{\theta_1, \theta_2, \theta_3\}$ is a vector of unknown parameters. The known values of ζ can then be used to determine the pressure head at any time following a sudden valve closure from using the equation

$$h(t) = A \exp^{-\zeta\omega_n t} \sin(\omega_d t) \tag{4.2}$$

where A is the amplitude of the oscillation, ω_n is the natural frequency of the system, and $\omega_d = \omega_n\sqrt{(1-\zeta^2)}$. In Chapter 3, we considered Θ as a vector of deterministic variables, and estimated their values by a non-linear regression analysis of the error between the model predictions and available experimental data. While this analysis

*Khilqa, S., M. Elkholy, M. AlTofan, J. M. Caicedo, and M. H. Chaudhry (2019). Uncertainty Quantification for Damping in Transient Pressure Oscillations. *Journal of Water Resources Planning and Management,* http://doi.org/10.1061/(ASCE)WR.1943-5452.0001089. Reprinted here with permission from ASCE

provides an estimate of the rate of decay of the pressure head, the model does not give the uncertainty of the predictions. That is, Eq. 4.1 result in a single value of damping for a set of Re_0, Ma and D/L. This value of ζ yields a single value of $h(t)$ for each time t without providing the possible variations of the prediction. Ideally, the model should provide the uncertainty associated with the prediction of $h(t)$. This prediction would be helpful for risk analysis and decision making. For example, a probabilistic model could be used to estimate the probability that the pressure head would be higher than a particular value of interest.

In this paper, Θ is expressed as a vector of random variables. The joint probability density function of these parameters is estimated using Bayesian inference (a brief introduction to the terms is given in the next section) and using the experimental data discussed in chapter 3. The joint distribution is described by the probability density considering all parameters (Θ), rather than independent distributions for each parameter (Ang and Tang, 2007). The resulting joint distribution from the analysis is then used for probabilistic predictions of the pressure head after the valve is suddenly closed. This estimates the probability density function of $h(t)$ for any value of t. Bayesian inference has been applied to estimate uncertainty in a variety of settings, including updating structural models (Beck and Katafygiotis, 1998; Katafygiotis and Beck, 1998), damage identification in structural systems (Behmanesh et al., 2017; Ching and Beck, 2004), leak detection in piping systems (Poulakis et al., 2003; Puust et al., 2008), hydrology (Thyer et al., 2009), droughts (Kim et al., 2017) and the calibration of water distribution models (Kapelan et al., 2007), among others.

4.2 Statistical inference

Before describing the Bayesian methodology used in this study, a number of terms in Bayes inference are introduced, readers interested in more details should see Beck and Katafygiotis (1998), Gelman et al. (2014), and Jaynes (2003). Uncertainty (or

lack of certainty) limits our capability to model a system. Uncertainty is classified as aleatory (or Type I) and epistemic (or Type II). Epistemic uncertainty stems from the gaps of knowledge while aleatory uncertainty is attributed to unknown variations when an experiment or physical phenomenon is repeated. Within a modeling context, the assumptions made during the development of a model, such as the assumed boundary conditions and material characteristics, result in epistemic uncertainty. Aleatory uncertainty is often modeled as a random variable added to the output of a model and it is used to express the "normal variation" observed when the same experiment is performed more than once. Although some believe that system parameters should be modeled considering both aleatory and epistemic uncertainty (Der Kiureghian and Ditlevsen, 2009), others believe that all uncertainty is epistemic and that uncertainty can always be reduced by learning more about the system.

Currently, there are two main statistical approaches based on how probability is defined. These two different approaches result in different methods to determine the probability of model parameters based on experimental data. Probability in a frequentist sense is understood as the chances that an event will occur. Parameters have a "true" value, and measurements are the outcomes of a random variable describing this parameter. For example, in the context of a single piping system discussed in this paper, the damping ratio ζ has a "true" value when analyzed from a frequentist perspective, and the uncertainty associated with its estimation should consider both epistemic and aleatory uncertainty. The epistemic aspects of the uncertainty could be reduced by performing more experiments and discovering new knowledge about the system. However, uncertainty can only be decreased to certain extend because aleatory uncertainty is always present.

Probability from a Bayesian perspective is interpreted as a state of knowledge. Random variables express our knowledge about the model parameters rather than expressing their "true" values. In this perspective, uncertainty is only epistemic and

can always be reduced by increasing our knowledge. Measurements are not viewed as the outcome of a random variable but as observations of the system. Bayesian analysis was first published by Thomas Bayes in 1763. Recently, it has been applied to problems in different domains after the seminal work by Jaynes (2003). Prior knowledge about the problem at hand plays an important role in Bayesian inference. Data is not analyzed in a vacuum from the analysts' beliefs; rather, data is used to update the belief of the analyst and the result of the analysis summarizes both the experience of the analyst and new knowledge provided by the data. Arguably, Bayesian probability provides a way to utilize the expertise of the analyst, which can be significant in engineering fields where experts have developed knowledge about the system behavior based on their prior work. However, it is to note that expressing this prior knowledge should be made with care. Otherwise, the results of the analysis could be biased. However, since the analyst's experience is utilized, it is possible to estimate model parameters based on data from only a few experimental values. The ability to estimate probabilities with few experiments is of particular interest for large systems because the experimental data from these real-life systems can be difficult and expensive to obtain.

Overall both Frequentist and Bayesian approaches are important and are suitable for statistical analysis (Bayarri and Berger, 2004). Bayesian method allows the use of prior knowledge engineering judgment. In contrast, the frequentist approach is not based on prior knowledge and lets the data "speak for itself". In this work, a Bayesian approach is adopted to for a probabilistic model for the dissipation ratio, ζ, for transient pressure oscillations.

4.3 Bayes inference

Bayesian inference is based on the Bayes theorem expressed by the equation (Bayes and Price, 1763):

$$P(\Theta|\Delta,\zeta) = \frac{P(\zeta|\Theta,\Delta)\ P(\Theta|\Delta)}{P(\zeta)} \tag{4.3}$$

where $\Delta = \{\mathrm{Re}_0, \mathrm{Ma}, \mathrm{D/L}\}$ and ζ represents the experimental data; $P(\Theta|\Delta,\zeta)$ is the posterior probability density function (PDF), which is the updated belief of the probability of the model parameters Θ given the experimental data Δ and ζ. $P(\zeta|\Theta,\Delta)$ is the likelihood PDF. $P(\Theta|\Delta)$ is the prior PDF and expresses the prior knowledge about the parameters. Note that this prior distribution is conditional to the range of values of Δ; $P(\zeta)$ is the model evidence and, in some cases, it is treated as a normalization constant for convenience. Instead of assuming a distribution for the posterior, a distribution is drawn based on the prior distribution, an assumed distribution of the likelihood, and the data. Even though prior distribution affects the posterior, it does not constrain the posterior to be a specific type of PDF. For example, assuming a Gaussian distribution for $P(\Theta|\Delta)$ does not limit $P(\Theta|\Delta,\zeta)$ to follow a Gaussian distribution. Furthermore, assuming a prior distribution where the parameters θ_1, θ_2 and θ_3 are uncorrelated does not constrain the covariance matrix of the joint posterior distribution to be diagonal. The posterior indicates correlation between parameters if supported by the data and the model.

4.4 Methodology

The methodology followed in this paper may be summarized as a three-step approach (Gelman et al., 2014): (1) develop models for the prior distribution; (2) update the model parameters; and (3) perform a posterior prediction check of the developed model. For this purpose, the experimental data is divided into three groups. Because of the limited number of experimental data sets, most of the experiments are used

to inform the prior PDF and update the model. Therefore, the first group of data (Δ_a, ζ_a) is from six experiments and is used to inform the prior distributions. This group includes at least one experiment with value of Re_0 greater than 31,000 to make sure that the prior PDF is informed using laboratory and field data. The specific tests to be used are selected randomly from the available tests. The second group (Δ_b, ζ_b) is used to update the parameters and includes nine experiments. The third group (Δ_c, ζ_c) is used to validate the model predictions and consists of two experiments. This group is also forced to have data for Re_0 greater than 31,000. This allows checking that the models are able to predict both small (laboratory) and large (project) experiments. The overall process of informing the prior PDF, updating the model, and performing the posterior predictive check is repeated three times to confirm that the model is validated regardless of which data was used for each data set. Tables 4.1, 4.2 and 4.3 list the characteristics of each experiment for each of the three trials. The value of ζ_{bf} in these tables are obtained by optimizing the value of ζ from Eq. 4.2 such that the values of $h(t)$ match the measured experimental pressure head. The values of ζ_{bf} are considered as the observed values in the Bayesian analysis.

The likelihood function needed in Eq. 4.3 is assumed to be a normal distribution defined by the equation

$$P(\zeta|\Theta,\Delta) = \frac{1}{\sqrt{2\pi\sigma_l^2}} exp(-\frac{(\zeta_{bf} - \zeta(\Theta, \mathrm{Re}_0, \mathrm{Ma}, D/L))^2}{2\sigma_l^2}) \tag{4.4}$$

where $\zeta(\Theta, \mathrm{Re}_0, \text{etc.})$ is as defined in Eq. 4.1. The standard deviation of the likelihood, σ_l, may be considered as a free parameter and added to the list of unknown parameters to be estimated. Therefore, in the reminder of this paper, $\Theta = \{\theta_1, \theta_2, \theta_3, \sigma_l\}$.

Prior PDF $P(\Theta|\Delta)$ may be defined by eliciting information from an expert (O'Hagan, 1998; Garthwaite et al., 2005), defining uninformative priors (Jaynes, 2003), or using past information. The prior distribution is assumed as a multinomial distribution of independent parameters. $P(\theta_i)$ follows a Normal distribution with parameters estimated using the first set of experiments, Δ_a. The mean, μ_{θ_i}, is estimated using a

Table 4.1: Data sets for the first trial

Test no.	Re_0	Ma	D/L	ζ_{bf}
Data to inform the prior PDF (Δ_a, ζ_a)				
1	7,845	2.58×10^{-4}	1.60×10^{-4}	0.014
4	4,348	1.49×10^{-4}	1.60×10^{-4}	0.016
8	5,731	2.68×10^{-4}	1.63×10^{-4}	0.016
17	239,957	7.75×10^{-4}	6.24×10^{-5}	0.029
12	8,398	1.36×10^{-4}	6.84×10^{-4}	0.008
9	10,635	5.08×10^{-4}	1.63×10^{-4}	0.017
Data for updating (Δ_b, ζ_b)				
2	6,482	2.10×10^{-4}	1.60×10^{-4}	0.014
11	8,398	1.36×10^{-4}	3.70×10^{-4}	0.007
3	7,876	2.55×10^{-4}	1.60×10^{-4}	0.013
7	4,918	1.72×10^{-4}	1.60×10^{-4}	0.017
10	6,160	4.03×10^{-4}	2.03×10^{-4}	0.017
13	7,207	1.81×10^{-4}	7.04×10^{-4}	0.007
14	31,000	2.68×10^{-4}	1.67×10^{-3}	0.010
6	5,410	1.80×10^{-4}	1.60×10^{-4}	0.016
5	5,597	1.91×10^{-4}	1.60×10^{-4}	0.016
Data for validation (Δ_c, ζ_c)				
16	136,139	4.37×10^{-4}	6.24×10^{-5}	0.022
15	97,584	3.13×10^{-4}	6.24×10^{-5}	0.018

nonlinear fitting of the model and the standard deviation σ_{θ_i} is estimated using a coefficient of variation of 0.4. The parameters of the prior distribution for each of the three trials are listed in Table 4.4. A Normal or Gaussian distribution is adopted because this distribution maximizes the entropy when the normal and standard deviation can be approximated (Jaynes, 2003); that is, it includes the least information about the problem, allowing the data to shape the posterior distribution. An inverse gamma distribution is adopted for $P(\sigma_l)$ because the standard deviation is a positive number and the inverse gamma distribution supports positive numbers only. This distribution has two parameters: shape α and scale β. The value of α is chosen by trial and error and is set equal to 3.1 for all the three trials. The value of β is found as the mean squared error of the fitting process to find the prior PDFs for θ_1, θ_2, and

Table 4.2: Data sets for the second trial

Test no.	Re_0	Ma	D/L	ζ_{bf}
Data to inform the prior PDF (Δ_a, ζ_a)				
1	7,845	2.58×10^{-4}	1.60×10^{-4}	0.014
17	239,957	7.75×10^{-4}	6.24×10^{-5}	0.029
9	10,635	5.08×10^{-4}	1.63×10^{-4}	0.017
3	7,876	2.55×10^{-4}	1.60×10^{-4}	0.013
10	6,160	4.03×10^{-4}	2.03×10^{-4}	0.017
11	8,398	1.36×10^{-4}	3.70×10^{-4}	0.007
Data for updating (Δ_b, ζ_b)				
14	31,000	2.68×10^{-4}	1.67×10^{-3}	0.010
4	4,348	1.49×10^{-4}	1.60×10^{-4}	0.016
12	8,398	1.36×10^{-4}	6.84×10^{-4}	0.008
13	7,207	1.81×10^{-4}	7.04×10^{-4}	0.007
5	5,597	1.91×10^{-4}	1.60×10^{-4}	0.016
2	6,482	2.10×10^{-4}	1.60×10^{-4}	0.014
6	5,410	1.81×10^{-4}	1.60×10^{-4}	0.016
7	4,918	1.72×10^{-4}	1.60×10^{-4}	0.017
8	5,731	2.68×10^{-4}	1.63×10^{-4}	0.016
Data for validation (Δ_c, ζ_c)				
15	97,584	3.13×10^{-4}	6.24×10^{-5}	0.018
16	136,139	4.37×10^{-4}	6.24×10^{-5}	0.022

θ_3. The values of β are 0.00199, 0.00058 and 0.00161 for the first, second and third attempts, respectively.

4.5 Sampling the posterior

Markov Chain Monte Carlo (MCMC) are used to draw samples from the posterior distribution. Markov chains are sequences of random variables $\Theta(1)$, $\Theta(2)$, ... $\Theta(k)$ where the probability of $\Theta(k)$ only depends on $\Theta(k-1)$. MCMC methods produce Markov chains that have a distribution that converges to that of the distribution being sampled. A number of MCMC methodologies are reported in the literature, including Metropolis-Hastings (Metropolis et al., 1953; Chib and Greenberg, 1995),

Table 4.3: Data sets for the third trial

Test no.	Re_0	Ma	D/L	ζ_{bf}
Data to inform the prior PDF (Δ_a, ζ_a)				
5	5,597	1.91×10^{-4}	1.60×10^{-4}	0.016
3	7,876	2.55×10^{-4}	1.60×10^{-4}	0.013
2	6,482	2.10×10^{-4}	1.60×10^{-4}	0.014
14	31,000	2.68×10^{-4}	1.67×10^{-3}	0.010
8	5,731	2.68×10^{-4}	1.63×10^{-4}	0.016
16	136,139	4.37×10^{-4}	6.24×10^{-5}	0.022
Data for updating (Δ_b, ζ_b)				
7	4,918	1.72×10^{-4}	1.60×10^{-4}	0.017
6	5,410	1.81×10^{-4}	1.60×10^{-4}	0.016
10	6,160	4.03×10^{-4}	2.03×10^{-4}	0.017
9	10,635	5.08×10^{-4}	1.63×10^{-4}	0.017
4	4,348	1.49×10^{-4}	1.60×10^{-4}	0.016
1	7,845	2.58×10^{-4}	1.60×10^{-4}	0.014
13	7,207	1.81×10^{-4}	7.04×10^{-4}	0.007
11	8,398	1.36×10^{-4}	3.70×10^{-4}	0.007
12	8,398	1.36×10^{-4}	6.84×10^{-4}	0.008
Data for validation (Δ_c, ζ_c)				
17	239,957	7.75×10^{-4}	6.24×10^{-5}	0.029
15	97,584	3.13×10^{-4}	6.24×10^{-5}	0.018

Table 4.4: Priors for trial

Trial	Parameter	μ_{θ_i}	σ_{θ_i}
1	θ_1	0.070	0.0280
	θ_2	0.600	0.2400
	θ_3	-0.030	0.0120
2	θ_1	0.038	0.0152
	θ_2	0.704	0.2816
	θ_3	-0.144	0.0576
3	θ_1	0.038	0.0152
	θ_2	0.704	0.2816
	θ_3	-0.144	0.0576

Gibbs sampling (Tanner and Wong, 1987), Hamiltonian MCMC (Neal et al., 2011), NUTS (Hoffman and Gelman, 2014) and many others. In this paper, Gibbs sampling is used to draw MCMC chains of 1×10^6 samples. The first 10000 samples of the chain are not considered to let the chain reach its equilibrium. Furthermore, one of each 7 subsequent samples are used for the analysis. A Z-score (Geweke et al., 1991) is used to check the convergence of the chains to stationarity. This convergence diagnostic metric identifies if sufficient numbers of samples have been drawn to describe the posterior distribution. Typical values of these scores are shown in Fig. 4.1. A chain is considered to have converged if the value of the Z-score is between ± 2.

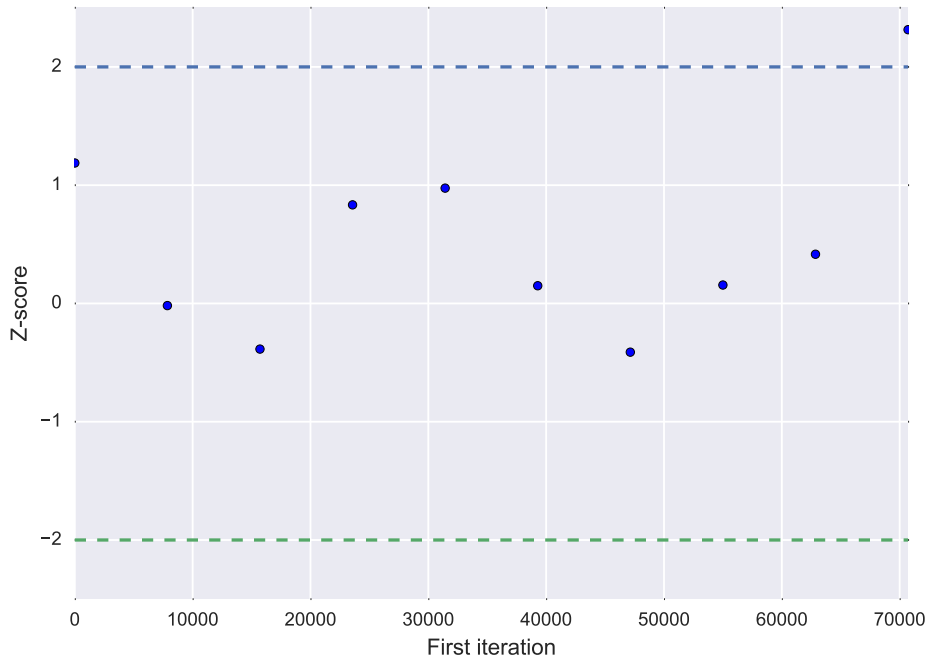

Figure 4.1: Z-score for θ_3

4.6 Posterior predictions

The probability of a new value of damping ratio, $\tilde{\zeta}$, may be used by marginalizing all the other values of the model,

$$P(\tilde{\zeta}) = \int P(\tilde{\zeta}, \Theta, \Delta) \mathrm{d}\theta = \int P(\tilde{\zeta}|\Theta, \Delta) P(\Theta) \mathrm{d}\Theta \tag{4.5}$$

However, the posterior distribution may be used to describe the probability of Θ. Therefore,

$$P(\tilde{\zeta}|\zeta, \Delta) = \int P(\tilde{\zeta}|\Theta, \Delta) P(\Theta|\zeta, \Delta) \mathrm{d}\Theta \tag{4.6}$$

Eq. 4.6 corresponds to the probability of an estimated damping ratio $\tilde{\zeta}$ given the experimental data utilized for updating and the characteristics of the system, Δ, and it is often called the posterior predictive distribution (Gelman et al., 2014). This estimation is conditional to the prior observations of ζ and the characteristics of the system, Δ. $P(\Theta|\zeta, \Delta)$ is the posterior PDF defined by Eq. 4.3, and $P(\tilde{\zeta}|\Theta, \Delta)$ is the likelihood function (Eq. 4.4) evaluated in $\tilde{\zeta}$. The quality of the model is assessed by predicting the values of the data for validation, ζ_c, given the parameters of those systems (Δ_c) and comparing the prediction with the experimental damping ratio. The posterior prediction of $\tilde{\zeta}$ is also used to estimate the values of pressure head $\tilde{h}(t)$ from Eq. 4.2.

4.7 Results and Discussion

The posterior for the second trial (See Table 4.2) is shown in Fig. 4.2 and is found to be similar to the other trials. The figures in the diagonal are the marginal distributions for each parameter while the figures off the diagonal show the pairwise PDF relationship between the two variables. The parameters are not independent when the shape of the plot between the two parameters is close to an oval. That is, the probability of the value of one parameter is conditional to the probability of the

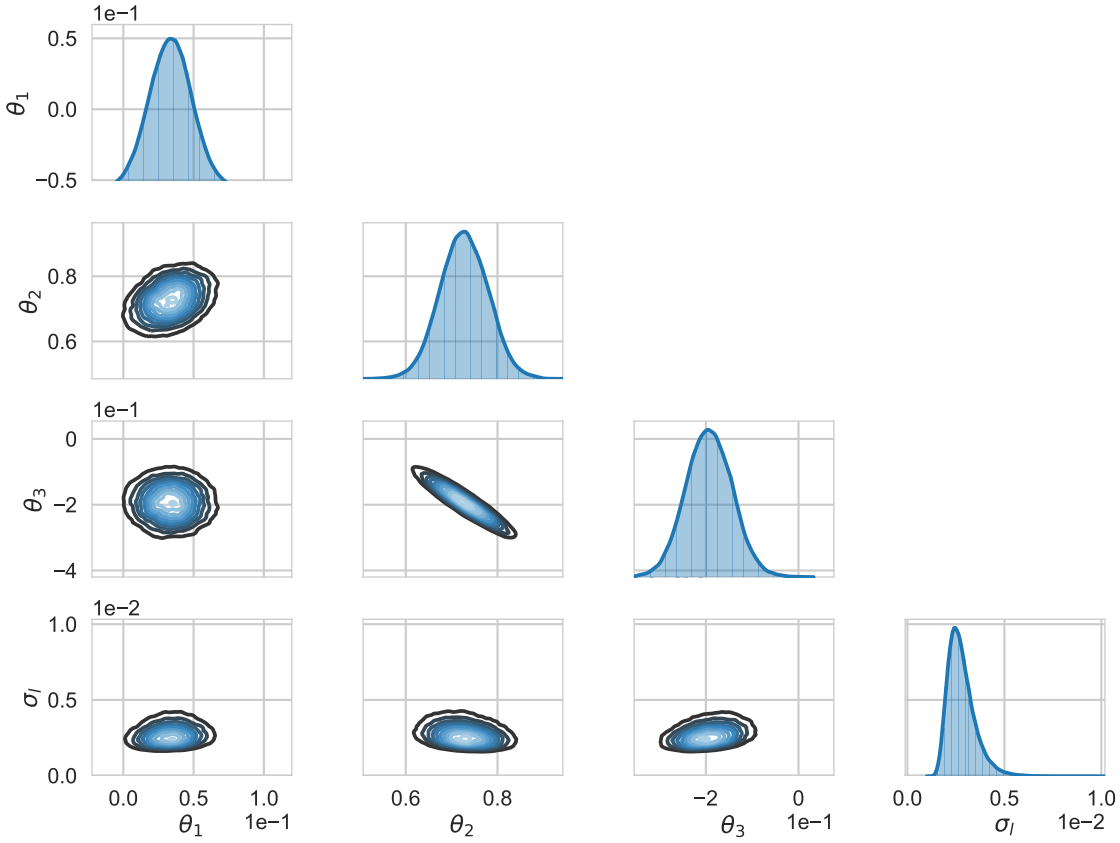

Figure 4.2: Posterior distributions of σ_l, θ_1, θ_2 and θ_3 for the second trial

value of the second parameter. When the shape is closer to a circle, the parameters are independent. The posterior shows a strong inverse relationship between θ_3 and θ_2 with correlation coefficient of -0.94 indicating that the model could be further simplified. (The other trails are shown in appendix C).

Figure 4.3 shows the posterior prediction of ζ for the three tests used for the validation. The experimental data is shown by a continuous vertical line and the 95% highest posterior density interval (HPD) is shown by the dashed lines. The HPD (or credible interval) is equivalent to the confidence intervals in a frequentist approach. This is, the dashed lines indicates the region where there is a 95% change for the value of ζ. The range of the 95% HPD depends on the values of Δ for each experiment. In some cases, such as Test 17 [Fig. 4.3(c)], the uncertainty in the prediction is larger than that in the other tests, such as Tests 15 and 16 [Fig. 4.3(a and b)]. The range of

95% HPD varies from approximately 1% to 6% depending on the test. This level of uncertainty is not surprising because of the difficulty in estimating the damping ratios, as reported in the literature (Hernandez and Nestor, 2016). Nevertheless, knowing the uncertainty in the estimation provides engineers operating large pipe systems with additional information—for example, the probability that a certain critical value of pressure head oscillation might be surpassed, as described later in the paper. All of the experimental data falls within the 95% HPD, indicating that the probabilistic model predicts the value of ζ satisfactorily with the available data. While in some cases the experimental value of ζ is close to the peak of the posterior prediction density [e.g., Fig. 4.3(a and b)], the peak of the PDF and the experimental value do not completely match those in [Fig. 4.3(c)]. The shape of the posterior prediction density also changes with the values of Δ. The shape of the posterior prediction density also changes with the values of Δ, and these shapes of Tests 15 and 16 are somewhat symmetric while the shape of the posterior prediction for Test 17 is not symmetric. This is reasonable since the damping ratio cannot be negative and higher skewness would be expected for smaller values of damping. In addition, the mean of the posterior prediction of ζ is higher than the experimental damping ratio values in these three tests. This indicates that the model is biased towards producing high values of damping ratio.(ζ distributions predicted by the model for all trails are shown in appendix C).

Figures 4.4 (a and b) show the predicted pressure head for Tests 16 and 17. The shaded region is the predicted 95% HPD using the model and the dots represent the experimental data. These tests are for high Re_0. The model has limitations in predicting the pressure during the first half-cycle of the experimental data for Test 16 and Test 17. This is possibly due to errors in the estimation of the value of A in Eq. 4.2, which is considered a deterministic parameter in this study, or to the process of digitizing the data points from the literature. The 95% HPD prediction

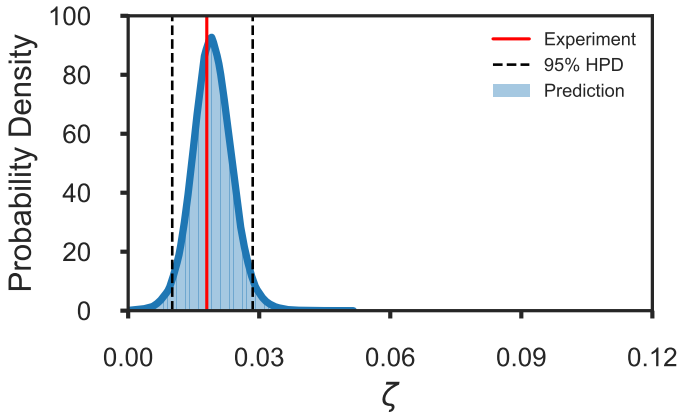

(a) Test 15

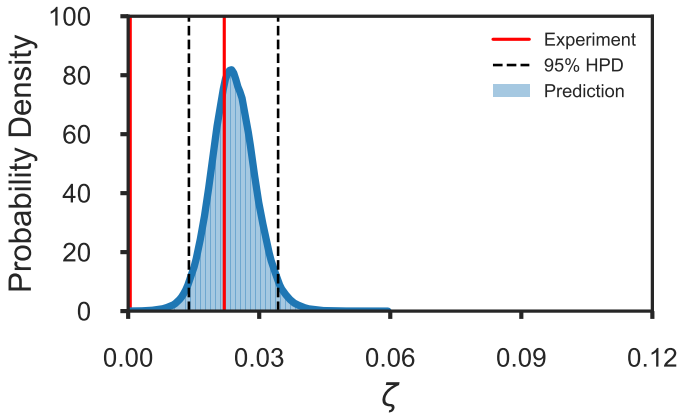

(b) Test 16

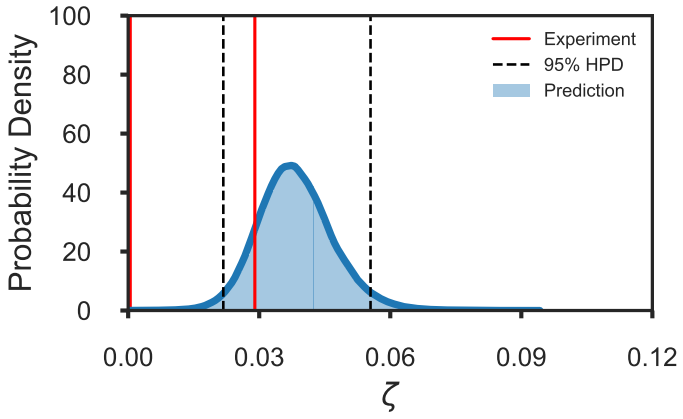

(c) Test 17

Figure 4.3: Distribution of ζ predicted by the model

represents the following cycles satisfactorily; then it becomes slightly off for the last few cycles. It is worth mentioning that the uncertainty in the prediction increases with time, expressed by a narrower band close to $t = 0$, and by a larger band towards the end of the record. The experimental data is close to the mid point between the upper and lower limits of the 95% HPD at the beginning of the experiment and close to the lower limit at the end.

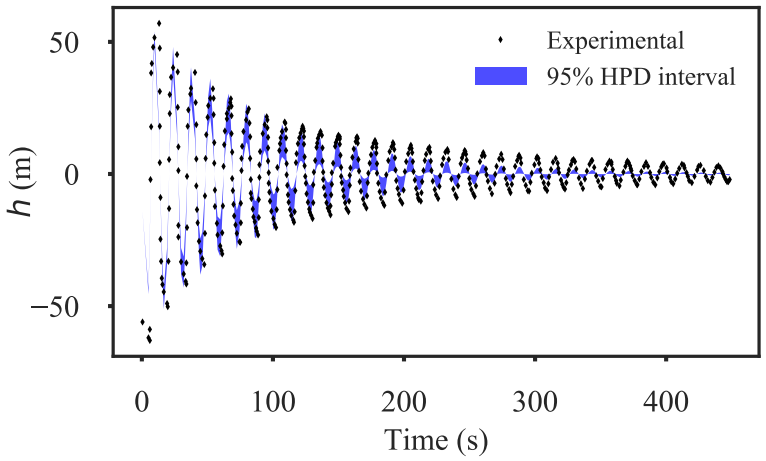

(a) Test 16

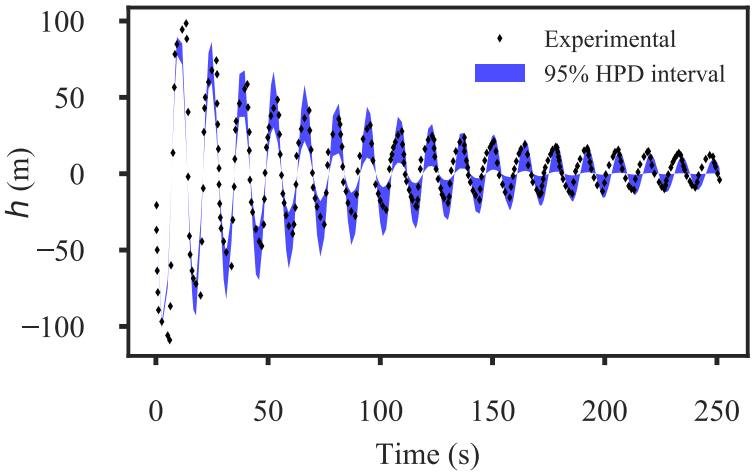

(b) Test 17

Figure 4.4: 95% HPD predicted by the model and experimental data

The probabilistic model may be used to make decisions for the operation of a piping system. For example, prediction of the dissipation of transient pressures is

needed to determine a suitable time for the second operation. The probability that the pressure head is less than a specific value may be determined from the MCMC chains and from the exponential decay of Eq. 4.2. By calculating the envelopes of the pressure oscillations from the exponential term in Eq. 4.2, and using the parameters of the probabilistic model developed in this study, it is possible to determine the time needed to restart a system. Fig. 4.5(a) hows the envelope of the predictions for the system of Test 16 drawn from the exponential term in Eq. 4.2, and Fig. 3.7(b) shows the probability of the pressure head being less than 10 m as a function of time. The MCMC chain is the same as that used to estimate 95 % HPD shown in Fig. 4.5(a) for Test 16. The probability shown in Fig. 4.5(b) increases as time passes and the pressure in the pipe decreases. Engineers may specify a reasonable level of probability to decide when to restart the system based on this value. For this particular test, the model shows that there is a 75% probability that $h \leq 10.00$ m after 130.0 seconds.

This work may be considered the seed for more future work on complex piping system. It would be a good idea to extend this study for such systems to obtain more reliable results with less chance of failure than those obtained using deterministic models.

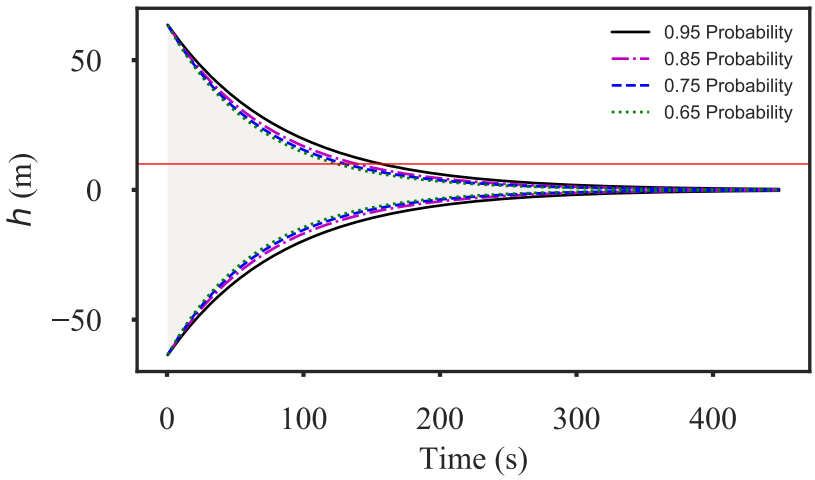

(a) Envelops of the pressure oscillation of Test 16

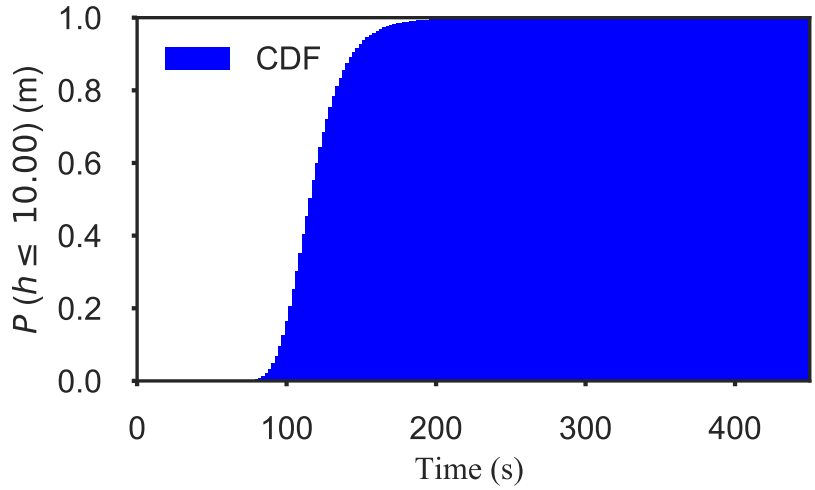

(b) Model application

Figure 4.5: 95% HPD predicted by the model and experimental data

Chapter 5

Applications of Instantaneous Acceleration-Based Models

5.1 Introduction

Since Daily et al. (1955) pointed out the difference between damping in the steady and unsteady flows, researchers have presented models that add significant amount to steady damping to match experimental or field data. Here, the unsteady friction models that include the unsteady friction term, J_u, such as Instantaneous-Acceleration-Based (IAB) models are discussed. In the following sections, an IAB model is considered for evaluating the effects of J_u on the attenuation of peaks and and the time variation of pressure head variations along a pipeline.

The governing equations for transient flows may be written as (Chaudhry, 2014)

Continuity equation

$$\frac{a^2}{g}\frac{\partial v}{\partial x} + \frac{\partial h}{\partial t} = 0 \tag{5.1}$$

Momentum equation

$$\frac{1}{g}\frac{\partial v}{\partial t} + \frac{\partial h}{\partial x} + J_s + J_u = 0 \tag{5.2}$$

where a = wave speed; g = gravitational acceleration; v = flow velocity; x = distance in the downstream x-direction along the pipe; t = time; h = pressure head in the pipe; $J_s = \dfrac{fv\,|v|}{2gD}$ = the steady friction term; f = Darcy's-Weisbach friction factor; D = the pipe diameter and J_u = the unsteady friction term. The one-coefficient IAB

model may be written as (Vítkovskỳ et al., 2006)

$$J_u = \frac{K}{g}\left(\frac{\partial v}{\partial t} + \text{Sign}\left(v\frac{\partial v}{\partial x}\right)\ a\frac{\partial v}{\partial x}\right) \tag{5.3a}$$

and for the two-coefficients IAB models as

$$J_u = \frac{1}{g}\left(K_{ut}\ \frac{\partial v}{\partial t} + K_{ux}\ \text{Sign}\left(v\frac{\partial v}{\partial x}\right)\ a\frac{\partial v}{\partial x}\right) \tag{5.3b}$$

where $K =$ is the decay coefficient for one-coefficient IAB model and K_{ut} and K_{ux} are the decay coefficients for the local and convective acceleration, respectively for two-coefficients IAB model. The relationship between the continuity and momentum equations may be written with the multiplier, λ, as

$$\lambda\ .\ (L_1 \equiv \text{Continuity eq.}) + (L_2 \equiv \text{Momentum eq.}) = 0 \tag{5.4}$$

Note that these coefficient are assumed constant with respect to time and space.

5.2 Two-Coefficients IAB model

In this case, combining Eqs. 5.1 to 5.3b with Eq. 5.4 for two-coefficients IAB model gives

$$\left[\frac{(1+K_{ut})}{g}\frac{\partial v}{\partial t} + \frac{K_{ux}.\phi.a + \lambda.a^2}{g}\frac{\partial v}{\partial x}\right] + \lambda\left[\frac{\partial h}{\partial t} + \frac{1}{\lambda}\frac{\partial h}{\partial x}\right] + J_s = 0 \tag{5.5}$$

in which, $\phi = sign\left(v\frac{\partial v}{\partial x}\right)$. If $h = h(x,t)$ and $v = v(x,t)$, then the total derivative

$$\frac{dv}{dt} = \frac{\partial v}{\partial t} + \frac{\partial v}{\partial x}\frac{dx}{dt} \tag{5.6a}$$

$$\frac{dh}{dt} = \frac{\partial h}{\partial t} + \frac{\partial h}{\partial x}\frac{dx}{dt} \tag{5.6b}$$

which when combined with Eqs. 5.1 and 5.2 gives,

$$\frac{dx}{dt} = \frac{K_{ux}.\phi.a + a^2\lambda}{1+K_{ut}} \tag{5.7a}$$

$$\frac{dx}{dt} = \frac{1}{\lambda} \tag{5.7b}$$

from which it follows that

$$\lambda = \frac{-K_{ux}\phi a. \pm \sqrt{{K_{ux}}^2 a^2 + 4a^2\left(1 + K_{ut}\right)}}{2a^2} \tag{5.8}$$

By dropping the higher terms, K_{ux}^2, and using a binomial expansion, λ for the case of tow-coefficients IAB model may be written as

$$\lambda = \frac{-K_{ux}.\phi \pm (2 + K_{ut})}{2a}$$

which gives inverse of the characteristic slope as

$$\frac{dx}{dt} = \frac{1}{\lambda} = \frac{2a}{-K_{ux}.\phi \pm (2 + K_{ut})} \tag{5.9}$$

The partial derivatives in unsteady friction term are approximated by finite-difference approximations on the characteristic grid. They are chosen such that they do not affect on adjacent computational sections and are therefore unaffected by proximity to the boundaries or pipe junctions. For this case, a condition has to be satisfied for the characteristic slope according to the sign of ϕ: If $\phi = 1$, then the slope, λ^+ is positive if $(K_{ut} + 2 - K_{ux} > 0)$. And as long as the slope, $dt/dx \geq 1/a$, the data from the previous time step are used to update the head and velocity at the next time interval. Moreover, if $\phi = -1$, then the solution is stable as long as the $K_{ut} \geq K_{ux}$.

Mathematically, the finite differences considered for each characteristic are as follows: The positive characteristic equation, C^+, may be written as

$$\frac{dv}{dt} + \frac{g\left(-K_{ux}\phi + 2 + K_{ut}\right)}{2a\left(1 + K_{ut}\right)}\frac{dh}{dt} + J_s * \frac{g}{(1 + K_{ut})} = 0 \tag{5.10}$$

which gives,

$$(v_P - v_L) + Cm_L\left(h_P - h_L\right) + J_s\frac{g}{1 + K_{ut}} = 0$$

or

$$v_P = v_L + Cm_L h_L + \frac{f v_L |v_L| g}{2D(1 + K_{ut})} - Cm_L.h_P \tag{5.11}$$

$$v_P = C_P - Cm_L.h_P \tag{5.12}$$

and the negative characteristic equation, C^-, as

$$\frac{dv}{dt} + \frac{g\left(-K_{ux}\phi - 2 - K_{ut}\right)}{2a\left(1 + K_{ut}\right)}\frac{dh}{dt} + J_s * \frac{g}{(1 + K_{ut})} = 0 \tag{5.13}$$

to give

$$v_P = v_R + Cm_R h_R + \frac{f v_R |v_R| g}{2D(1 + K_{ut})} - Cm_R.h_P \tag{5.14}$$

$$v_P = C_N - Cm_R.h_P \tag{5.15}$$

where, v_L and v_R are the velocities at the previous time step for the nodes on the left-and right-hand sides, respectively; h_P is the pressure head oscillation at the next time step, i.e., at $t + \Delta t$ and h_L and h_R are the head at the previous time step for the nodes on the left-and right-hand sides node, respectively;

$$Cm_L = \frac{g\left(-K_{ux}\phi + 2 + K_{ut}\right)}{2a\left(1 + K_{ut}\right)} \tag{5.16}$$

$$C_P = v_L + Cm_L h_L + \frac{f v_L |v_L| g}{2D(1 + K_{ut})} \tag{5.17}$$

$$Cm_R = \frac{g\left(-K_{ux}\phi - 2 - K_{ut}\right)}{2a\left(1 + K_{ut}\right)} \tag{5.18}$$

$$C_N = v_R + Cm_R h_R + \frac{f v_R |v_R| g}{2D(1 + K_{ut})} \tag{5.19}$$

The K_{ut} adjusts the temporal acceleration term to match the time variation of experimental and computed pressure head oscillations, while K_{ux} adjusts the convective acceleration term that produces the damping.

5.3 One-Coefficient IAB model

Following the same procedure as before, the multiplier for the one-coefficient IAB model equals to

$$\lambda = \frac{-k\phi \pm (K + 2)}{2a} \tag{5.20}$$

Then, the positive characteristic equation, C^+, may be written as

$$\frac{dv}{dt} + \frac{g(-K\phi + 2 + K)}{2a(1 + K)}\frac{dh}{dt} + J_s * \frac{g}{(1 + K)} = 0 \tag{5.21}$$

or as function of the unknown, v_P, as

$$v_p = C_p - C_{a_L} h_p \tag{5.22}$$

where

$$C_{a_L} = \frac{2g}{a\,(K\phi + K + 2)} \tag{5.23}$$

$$C_p = v_L + C_{a_L} h_L - R v_L |v_L| \tag{5.24}$$

and the negative characteristic equation, C^-, as

$$\frac{dv}{dt} + \frac{g(-K\phi - 2 - K)}{2a(1+K)} \frac{dh}{dt} + J_s * \frac{g}{(1+K)} = 0 \tag{5.25}$$

or as function of the unknown, v_P, as:

$$v_p = C_N - C_{a_R} h_p \tag{5.26}$$

where,

$$C_{a_R} = \frac{2g}{a\,(K\phi - K - 2)} \tag{5.27}$$

$$C_p = v_R + C_{a_R} h_R - R v_R |v_R| \tag{5.28}$$

$$R = \frac{f \Delta t}{2D\ \ (1+K)} \tag{5.29}$$

These coefficients in IAB models increase the amplitude of the pressure head by a factor of $(1 + K)$ at $t = 0$. This can be proof it mathematically as follows

Let $R = f/\,(2gD)$ and $Ca_L = g/a$. If $K = 0$ and $f = 0$, then $R = 0$.

For the case of downstream valve closure

$$h_P = \frac{C_P}{Ca_L} \tag{5.30}$$

$$h_P = \frac{V_o + Ca_L H_s}{Ca_L} \tag{5.31}$$

$$h_P = \frac{aV_o}{g} + H_s \tag{5.32}$$

where, the term aV_o/g represents the change in pressure head according to Joukowsky relationship.

Now, let's assume $K \neq 0$ and $f = 0$ and thereby $R = 0$. When $\phi = 1$, $Ca_L = \frac{g}{a(1+K)}$, which gives

$$C_p = v_R + Ca_L h_R - 0.0 \tag{5.33}$$

$$v_P = 0.0 \tag{5.34}$$

$$h_P = \frac{v_R + Ca_L h_R}{Ca_L} \tag{5.35}$$

$$h_P = \frac{V_o + \frac{g}{a(1+K)} H_s}{\frac{g}{a(1+K)}} \tag{5.36}$$

$$\Delta h = \frac{a(1+K)V_o}{g} \tag{5.37}$$

The IAB models multiply the amplitude Δh at $t = 0$ by $(1 + K)$ whether it is one-coefficient or two-coefficients models. In addition to the effect of one- or two-coefficients models on Joukowsky pressure rise, Δh as shown in Eq. 5.37, IAB models affect the natural frequency of the pipeline system by changing the wave speed and gravitational acceleration (Vítkovskỳ et al., 2006). They found that these changes are due to multiplying the gravitational acceleration g and wave speed a by $1/(1+K)$ and $1/\sqrt{1+K}$, respectively.

5.4 Discussion

Both one-coefficient and two-coefficients models are used to simulate the pressure head oscillations for each experiment listed in Tables 3.1 and 3.2. As mentioned earlier, the static head is subtracted from pressure head oscillation data; as a result, the pressure head oscillations are either positive or negative every $2L/a$. The wave speed for each data listed in 3.1 and 3.2 is the average value of the wave speed computed from $a = 1/N \sum_{i=1}^{N} (2L/t_i)$ by calculating the wave speed, $a_i = 2L/t_i$, for each half cycle, i.e., $2L/a$ during the entire simulation period of the measurements.

This wave speed represents the wave speed for the system even if there is entrained or trapped air in the piping system. The wave speed computed in this manner insures that the simulation results and the experimental measurements match in time. This may be shown by comparing the results of the one-coefficient and two-coefficients models, as shown in Fig. 5.1 a, where the values of these coefficients are equal. Therefore, hereinafter, K_{ux} and K_{ut} are referred to as k. In addition, this figure shows that the time variation between the experimental data and the computed results with either one-coefficient or two-coefficient match satisfactorily after the first few cycles, but it matches poorly during the last several cycles. This is expected because the one-coefficient or two-coefficients models adjust the wave speed as mentioned above. Another examples of the comparison are shown in Fig 5.1 b and c.

As mentioned above, data listed in Tables 3.1, 3.2 and Eqs 5.1, 5.2. are used to simulate pressure head oscillations; Test number 15, 16, and 17 are excluded. The reason for this exclusion is that the number of tests conducted in the laboratory is significantly greater than those for real-life applications. Note that these data are for the turbulent flow, elastic pipes material, and the boundary conditions are a closing valve either at the downstream end or at the upstream end.

In Table 5.1, k is determined by trial and error until the best fit between the experimental data and the computed results are obtained, f is the steady state Darcy-Weisbach friction factor. In the table, D_{J_s} and D_{J_s,J_u} are the percent of damping due to using only the steady friction, and both steady friction and unsteady friction together, respectively. The percent of damping of the former may be computed as the difference in area under the curve of the pressure head oscillations for frictionless system and the area of the pressure head oscillations using only the steady friction divided by the area under the curve for frictionless system.

Mathematically, this may be expressed as

$$Dj_s = \sum_{i=1}^{N} \left(\frac{\int |h_{j_o}| \, dt - \int |h_{j_s}| \, dt}{\int |h_{j_o}| \, dt} \right) \tag{5.38}$$

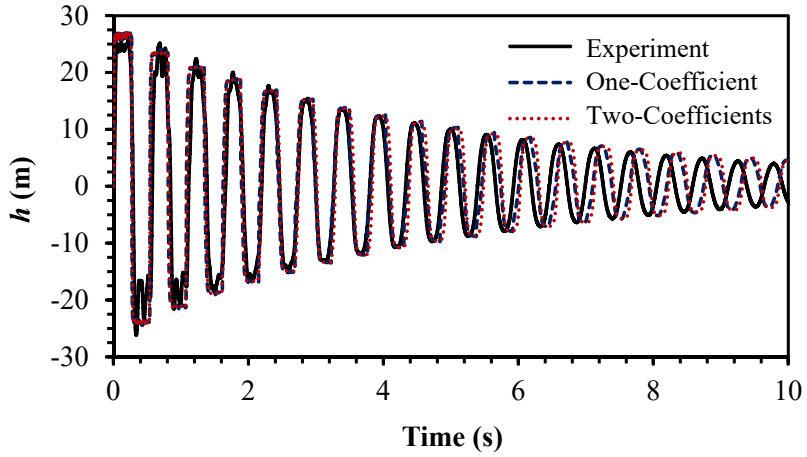

(a) Test no.6

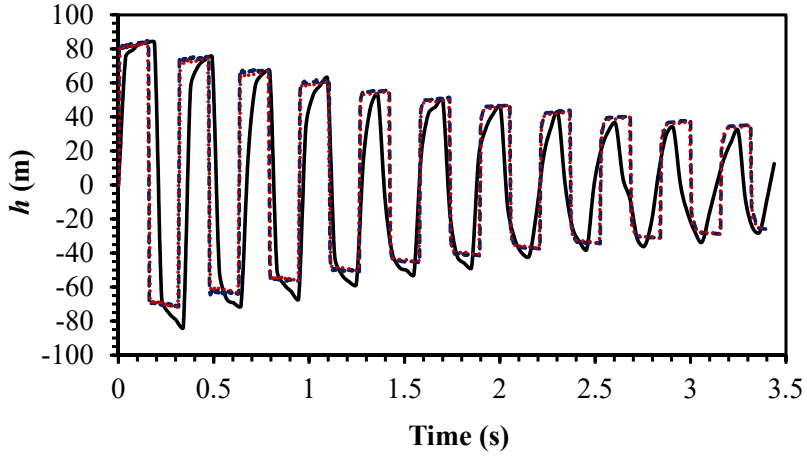

(b) Test no.9

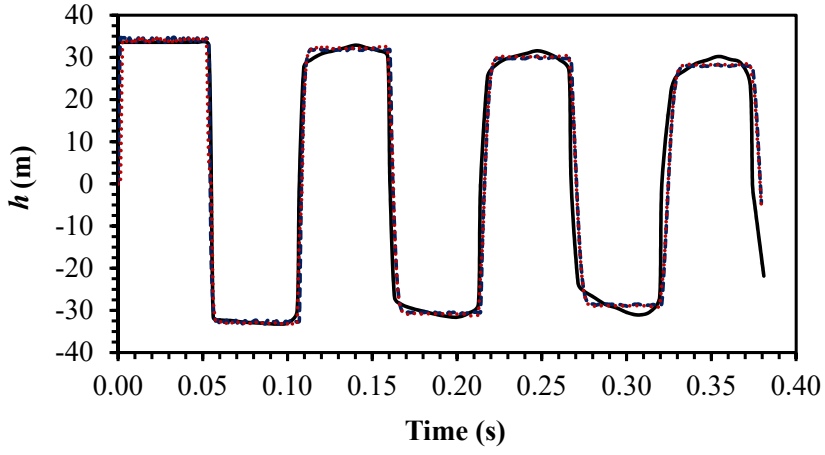

(c) Test no.13

Figure 5.1: Comparison of experimental and computed pressure oscillation by one-coefficient and two-coefficients models

Table 5.1: The values of k and other parameters related to the importance of unsteady friction

Test No.	k	f	D_{J_s}	D_{J_s,J_u}	D_{J_u}	Γ	P	I	S_c	Boundary action I.V.C*
1	0.040	0.033	0.350	0.668	0.318	0.48	6.83	0.053	25	D/S
2	0.041	0.035	0.387	0.728	0.341	0.47	8.15	0.046	33	D/S
3	0.035	0.033	0.468	0.776	0.308	0.40	6.90	0.053	42	D/S
4	0.064	0.039	0.374	0.827	0.453	0.55	10.86	0.036	39	D/S
5	0.049	0.036	0.440	0.827	0.387	0.47	8.84	0.043	45	D/S
6	0.045	0.037	0.397	0.777	0.379	0.49	9.21	0.042	38	D/S
7	0.050	0.038	0.384	0.776	0.392	0.50	9.40	0.041	36	D/S
8	0.040	0.036	0.220	0.432	0.212	0.49	6.40	0.059	11	D/S
9	0.020	0.031	0.307	0.430	0.082	0.21	3.65	0.097	11	D/S
10	0.065	0.0091	0.091	0.493	0.402	0.82	10.57	0.018	12	D/S
11	0.022	0.035	0.057	0.254	0.197	0.78	29.18	0.013	9	U/S
12	0.022	0.035	0.054	0.363	0.309	0.85	53.81	0.007	17	U/S
13	0.030	0.034	0.015	0.111	0.096	0.87	42.25	0.009	4	D/S
14	0.025	0.023	0.013	0.164	0.152	0.92	82.08	0.004	7	U/S

* = instantaneous valve closure.

N is the number of cycles of the pressure head-oscillations multiplied by two; h_{j_o} is the pressure computed by using the continuity and momentum equations, 5.1 and 5.2, for frictionless system, i.e., J_s and $J_u = 0$. The pressure head, h_{j_s}, is computed using Eqs., 5.1 and 5.2 that accounts for only friction losses due to steady state condition, i.e., $J_s \neq 0$ and $J_u = 0$, and dt is defined as the time step. The limit of the integrals is between two points on the time axis when the pressure head oscillations change from positive to negative and vise versa. The percent of damping due to using both steady and unsteady friction, D_{J_s,J_u}, is calculated from the following equation

$$D_{J_s,J_u} = \sum_{i=1}^{N} \left(\frac{\int |h_{j_o}| \; dt - \int |h_{j_s,j_u}| \; dt}{\int |h_{j_o}| \; dt} \right) \tag{5.39}$$

where h_{j_s,j_u} is the pressure head oscillation computed from the continuity and momentum equations that accounts for energy loss due to steady friction and unsteady friction, i.e., $J_s \neq 0$ and $J_u \neq 0$. $D_{J_u} = D_{J_s,J_u} - D_{J_s}$; Γ is the percent of damping due to unsteady friction relatively to the total damping due to both steady friction

and unsteady friction, i.e., $\Gamma = (D_{J_u}/D_{J_s,J_u})$; S_c stands for simulated cycles and is $4L/a_{\text{comp}}$, rounded to the nearest integer.

To study the significance of the assumption of unsteady friction as compared to steady friction in the modeling of transient flows, two dimensionless parameters are presented in the literature. The first one, P, indicates the acceptability of the steady assumption presented by Ghidaoui et al. (2002). P as defined in the earlier chapters is the ratio of radial diffusion time scale of vorticity, T_{dv}, to pipe core to time scale of the wave propagation from one end of the pipe to the other end, T_w (Zhao and Ghidaoui, 2004), and may be expressed mathematically as $P = 2D/(\sqrt{f}L\text{Ma})$. The second parameter, I, is presented by Duan et al. (2012) which is a lumped dimensionless parameter and indicates the relative importance of unsteady friction in transient flows. As I increases, unsteady friction losses decrease and ultimately becomes insignificant. This may be expressed mathematically as $I = f\text{Re}_0 T_w/T_d = f\text{Ma}\, L/D$.

Figure 5.2 shows the pressure oscillations following instantaneous valve closure for different tests to illustrate the percent of the damping due to steady and unsteady friction modeling on the damping of pressure oscillations as compared to a frictionless system and experimental data. It is clear from Fig. 5.2 a and b that the difference in the percent of the damping due to steady friction and unsteady friction modeling is significant. In addition, it is noticed in this figure that the effect of steady or unsteady friction on the damping is insignificant for the first or second pressure cycles. In other words, energy losses due to wall friction and convective acceleration are small during the first two cycles. Furthermore, the effect of unsteady friction on the damping becomes significant after the first two cycles. This means that for design purposes, first transient pressure peak in piping system is unaffected by dissipation as mentioned earlier in chapter 3.

Figure 5.3 shows the variation of k vs. Re_0 where k decreases as Re_0 increases.

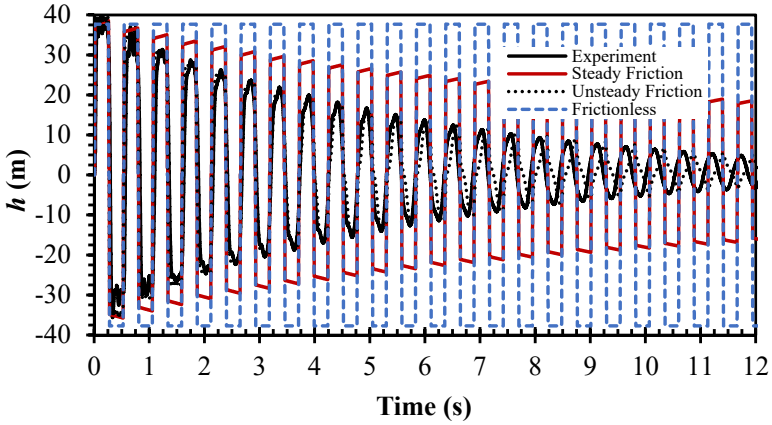

(a) Test no. 1

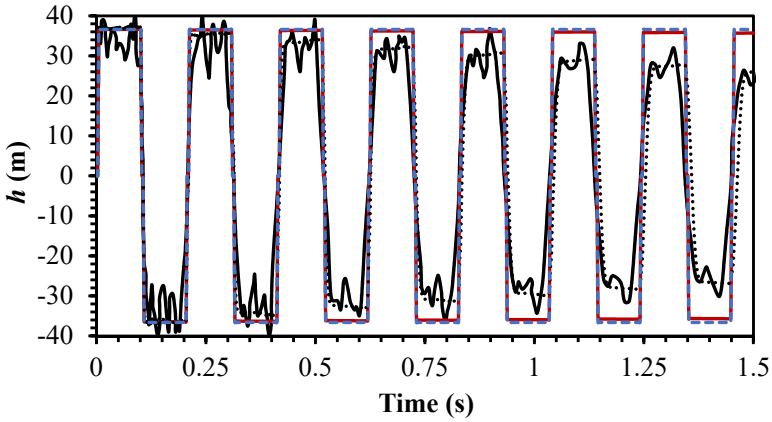

(b) Test no. 14

Figure 5.2: Comparison of experimental and computed pressures by different numerical models

This figure also shows that k depends on $\mathrm{Re}_0 \leq 10{,}635$. The range of k is between 0.020 and 0.065 for Re_0 ranging from 4348 to 10635. This is within the range mentioned in chapter 2. It is worth mentioning that Test no. 14 is neglected due to the gap in Re_0 where more data are needed to show the variation of k for $\mathrm{Re}_0 \geq 10{,}635$. At present, clear physical explanation for this behavior for the damping ratio is not available except that presented in the previous chapter. Even though Fig. 5.3 shows a defined relationship between Re_0 and k, it is not confirmed that this relationship may be applied for other systems due to the change in the structure of the flow during the transient state. In addition, k values are not indicative of the significance of

the damping due to unsteady friction. For example, for Test no. 13, the percent of damping due to unsteady friction, Γ, is 87% for k equals 0.03, while Γ is 48% for k equals 0.04 for Test no. 1.

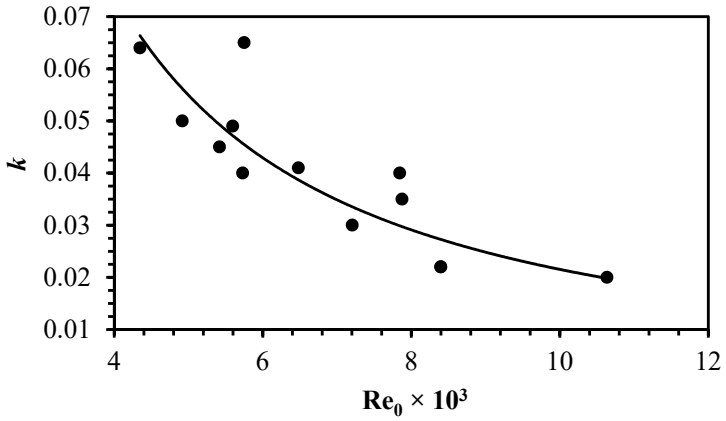

Figure 5.3: Re_0 vs. k

As mentioned earlier, P measures the acceptability of the steady assumption in the modeling of transient flow. Figure 5.4 shows the variation of k vs. P: For $P < 11$, k depends on P, while for $P > 29$, k appears to be constant. For the modeling of transient flows, Ghidaoui et al. (2002) indicated that the steady-state assumption is acceptable if $P \gg 1$. In this figure, $P > 29$, which confirms this assumption. However, the information is not sufficient to confirm that the steady-state assumption to model the transient flows is acceptable as shown in Fig. 5.4. The average values of k for $P > 29$ is approximately 0.025. This value does not indicate how much k contributes to the damping of the pressure oscillations, and thus, the acceptability of using steady-state assumptions for modeling transient flows is not confirmed for $P > 29$ in this figure. To further clarify this, Fig. 5.5 shows that there is no obvious defined relationship between k and its damping percent, Γ. Moreover, Fig. 5.6 shows that the damping due to unsteady friction, Γ, increases as P increases. This contradicts the findings of Ghidaoui et al. (2002).

It is a well-known fact that the velocity profiles change significantly during tran-

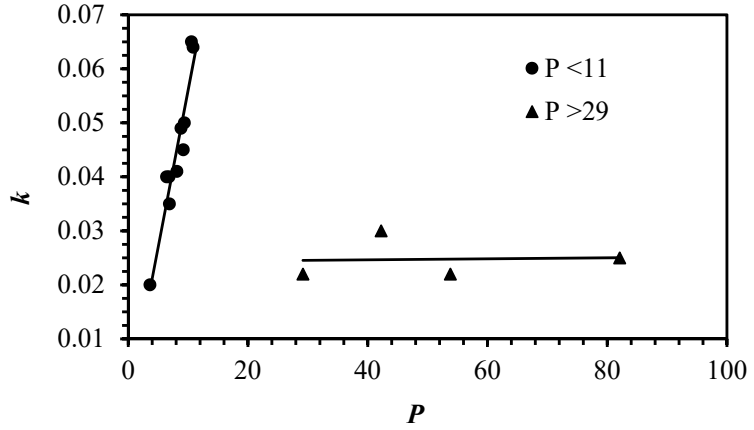

Figure 5.4: P vs. k

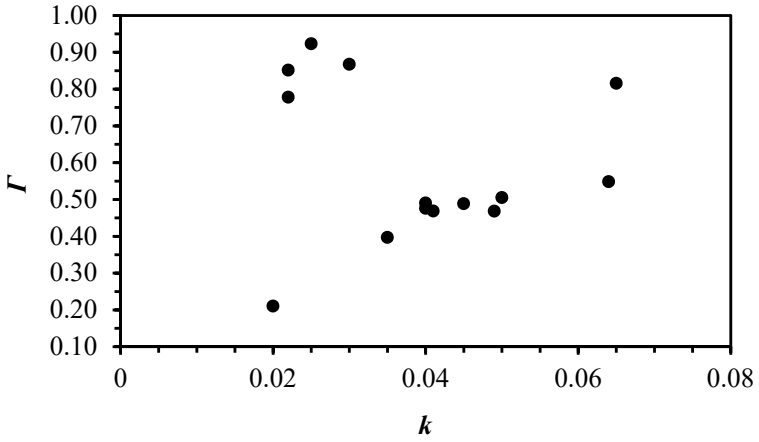

Figure 5.5: k vs. Γ

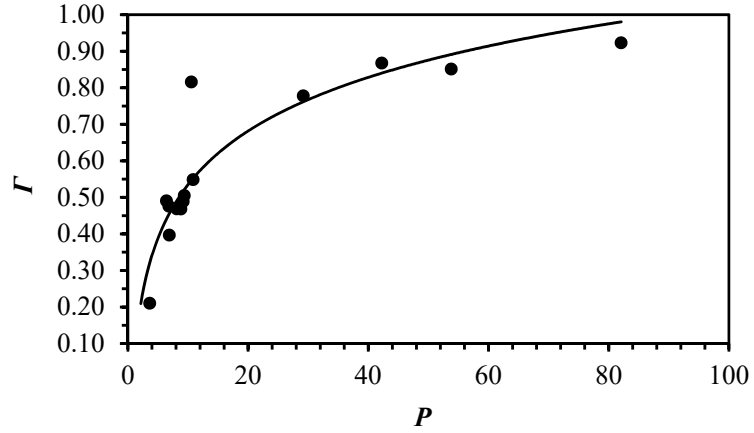

Figure 5.6: k vs. Γ

sient flows; typically flows near the wall and in the core move in the opposite directions and vortices form at the separation zones. This was pointed by Fox in the discussion of Plant et al. (1963) and confirmed by numerical modeling by several authors (Brunone et al. (1991, 2000); Silva-Araya and Chaudhry (1997); Vítkovskỳ et al. (2006)). Therefore, investigating the part of the damping due to unsteady friction during the transient may help to understand the phenomenon.

To indicate the percent of damping due to unsteady friction, Fig. 5.7 shows the variation of Γ vs. I. It is shown clearly that as I increases, Γ decreases. For example, for $I \leq 0.007$, $\Gamma \geq 85\%$, while for $I \geq 0.036$, $\Gamma \leq 55\%$. This confirms the finding of Duan et al. (2012).

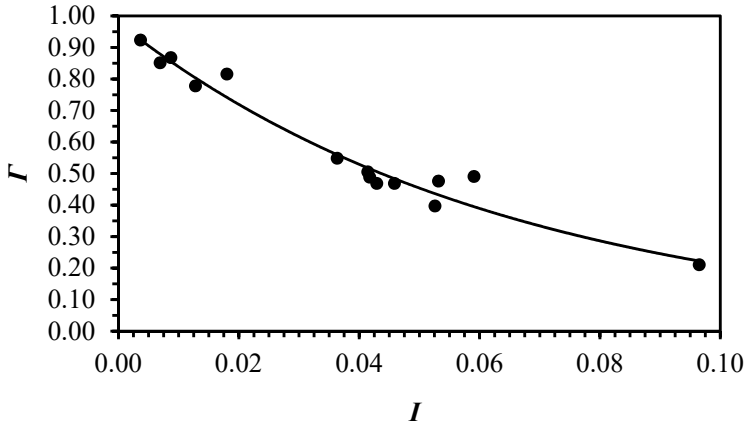

Figure 5.7: I vs. Γ

In chapter 3, the damping ratio, ζ_{bf} was introduced. As mentioned earlier, the damping ratio consists of steady and unsteady friction, and since the damping ratio is computed from pre-transient state, it is worth illustrating the variation of damping ratio vs. k. Figure 5.8 shows that as ζ_{bf} increases, k increases. In this figure, test no. 9 is excluded due to anomalous behavior. Furthermore, Fig. 5.9 shows the variation of ζ_{bf} vs. Γ which shows that as Γ increases, ζ_{bf} decreases. This behavior may explain that the damping due to unsteady friction may become insignificant in some transient pressurized flows conditions.

To conclude, the results shows that transient pressurized flows are complex and extremely rapid and making conclusions that fit for every cases are difficult. Therefore, additional experiments are needed to universally cover transient pressurized flows. Reynolds number, Mach number and D/L should have wide range with relatively small intervals for these investigations. These experiments include both real-life and laboratory systems.

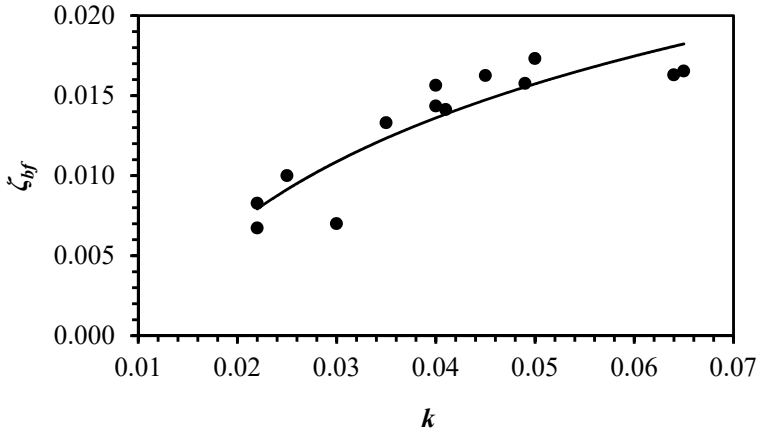

Figure 5.8: k vs. ζ_{bf}

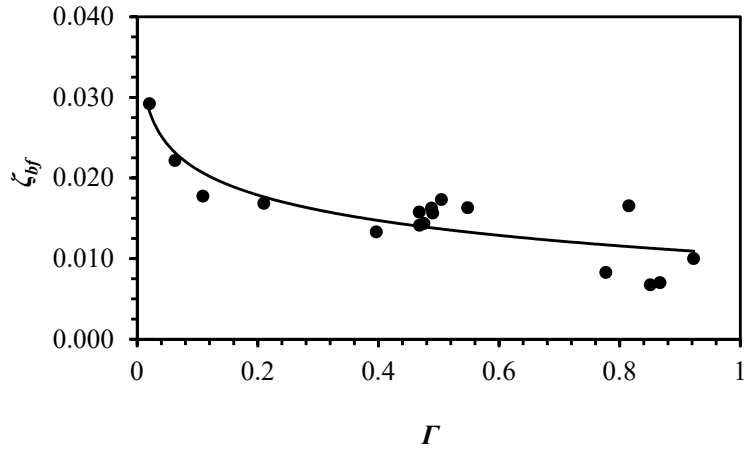

Figure 5.9: Γ vs. ζ_{bf}

Chapter 6

Summary and Conclusions

6.1 Damping in Transient Pressurized Flows

In addition to the maximum and minimum transient pressures in a piping system, the dissipation of the transient oscillations with time is important to initiate properly multiple operations in a system. This study presents the computation of damping of pressure oscillation in a simple piping system following the methodology used for the computation of the dissipation of vibrations of structures such as bridges, caused by impulse loading, such as earthquakes. A simple, reliable model to predict the dissipation of the pressure head oscillations is developed for the case of instantaneous valve closure as well as caused by gradual valve closure.

Conclusions are summarized as follows:

1. This model is not computationally intensive.
2. The model does not depend on the history of computed results.
3. The model does not require the simulation of the entire system.
4. Damping ratio is determined by using Reynolds number, Mach number, and the ratio of the diameter to the length of the pipe.
5. Damping ratio depends significantly on Reynolds number for, Re_0 greater than 40,000.
6. Damping ratio is linearly proportional with Mach number.

7. Damping ratio is inversely proportional to the ratio of the diameter to length of the pipe.

8. The length of the pipe plays an important role due to its effect on the frequency of the pipeline system.

9. The effect of relative roughness is small and may be neglected. The damping ratio obtained from the experiments varies from 0.007 to 0.017 for Reynolds number less than 40,000 and from 0.018 to 0.029 for higher Reynolds numbers.

10. The damping ratio increases significantly when the dimensionless parameter, P, between 0.8 to 10.

6.2 Uncertainty Quantification for Damping in Transient Pressurized Flows

A methodology is presented to estimate the uncertainty in a model to determine the dissipation of pressure oscillations in simple piping systems. The model developed uses a wide range of Re_0, Ma and D/L. The model parameters are updated using Bayesian inference and experimental data from laboratory and field studies. The resulting probabilistic model may be used to estimate the probability of the damping ratio and the pressure head oscillation for a pipeline following sudden valve closure. The probabilistic model is validated using data from field studies. The 95% highest posterior density of the predicted damping ratio includes the experimental data in the cases tested. The range of the 95% highest posterior density estimate of ζ is approximately between 1% and 6%. Lower values of damping appear to have lower variation than higher values of damping. The model is applied to determine the probability of the time for a specific pressure to occur in order to restart a system after transient condition produced by an earlier operation.

6.3 Applications of Instantaneous Acceleration Based Model

In this study, applications for Instantaneous Acceleration Based models are presented. This includes the one-coefficient and the two-coefficient models. For 14 different experiments, the unsteady friction are determined by trail and error to fit the experimental data. For Re_0 ranging between 4,348 to 31,000, the unsteady coefficient, k, is between 0.020 to 0.065. Using these models affect the natural frequency of the pipeline system by multiplying the magnitude of the wave speed and Joukowsky pressure rises as well. It is found that as Re_0 increases, the coefficient for unsteady friction decreases. The damping percent due to unsteady friction relatively to the total damping is computed by the area under the curves of the pressure oscillations. In addition, the percent of the damping due to unsteady friction is greater than 85% for a parameter, $I \leq 0.007$, which describes the importance of unsteady friction.

References

Abreu, J. and A. Almeida (2004). Wall shear stress and flow behavior under transient flow in a pipe. In *Proc., 9th Int. Conf. on Pressure Surges*, pp. 457–476. BHR Group Cranfield, UK.

Adamkowski, A. and M. Lewandowski (2006). Experimental examination of unsteady friction models for transient pipe flow simulation. *Journal of Fluids Engineering 128*(6), 1351–1363.

Ang, H. and W. H. Tang (2007). Probability concepts in engineering. *Planning 1*(4), 1–3.

Axworthy, D. H., M. S. Ghidaoui, and D. A. McInnis (2000). Extended thermodynamics derivation of energy dissipation in unsteady pipe flow. *Journal of Hydraulic Engineering 126*(4), 276–287.

Bayarri, M. J. and J. O. Berger (2004). The interplay of bayesian and frequentist analysis. *Statistical Science*, 58–80.

Bayes, M. and M. Price (1763). An essay towards solving a problem in the doctrine of chances. by the late rev. mr. bayes, frs communicated by mr. price, in a letter to john canton, amfrs. *Philosophical Transactions (1683-1775)*, 370–418.

Beck, J. L. and L. S. Katafygiotis (1998). Updating models and their uncertainties. i: Bayesian statistical framework. *Journal of Engineering Mechanics 124*(4), 455–461.

Behmanesh, I., B. Moaveni, and C. Papadimitriou (2017). Probabilistic damage identification of a designed 9-story building using modal data in the presence of modeling errors. *Engineering Structures 131*, 542–552.

Bergant, A., A. Ross Simpson, and J. Vìtkovsk (2001). Developments in unsteady pipe flow friction modelling. *Journal of Hydraulic Research 39*(3), 249–257.

Bergant, A. and A. Simpson (1994). Estimating unsteady friction in transient cavitating pipe flow. In *Proc. 2nd Int. Conf. on Water Pipeline Sys., BHR Group, Edinburgh, U.K.*, pp. 3–16. Mechanical Engineering Publications Limited.

Bergant, A., A. S. Tijsseling, J. P. Vítkovskỳ, D. I. Covas, A. R. Simpson, and M. F. Lambert (2008a). Parameters affecting water-hammer wave attenuation, shape and timing-part 1: Mathematical tools. *Journal of Hydraulic Research 46*(3), 373–381.

Bergant, A., A. S. Tijsseling, J. P. Vítkovskỳ, D. I. Covas, A. R. Simpson, and M. F. Lambert (2008b). Parameters affecting water-hammer wave attenuation, shape and timing-part 2: Case studies. *Journal of Hydraulic Research 46*(3), 382–391.

Brunone, B., M. Ferrante, and M. Cacciamani (2004). Decay of pressure and energy dissipation in laminar transient flow. *Journal of fluids engineering 126*(6), 928–934.

Brunone, B., U. Golia, and M. Greco (1991). Some remarks on the momentum equation for fast transients. In *Proc. Int. Conf. on Hydr. Transients With Water Column Separation*, pp. 201–209.

Brunone, B., B. W. Karney, M. Mecarelli, and M. Ferrante (2000). Velocity profiles and unsteady pipe friction in transient flow. *Journal of water resources planning and management 126*(4), 236–244.

Bughazem, M. and A. Anderson (1996). Problems with simple models for damping in unsteady flow. In *BHR Group Conference Series Publication*, Volume 19, pp. 537–548. Mechanical Engineering Publications Limited.

Bughazem, M. and A. Anderson (2000). Investigation of an unsteady friction model for waterhammer and column separation. In *BHR Group Conference Series Publication*, Volume 39, pp. 483–498. Bury St. Edmunds; Professional Engineering Publishing; 1998.

Carlsson, J. (2016). Water hammer phenomenon analysis using the method of characteristics and direct measurements using a" stripped" electromagnetic flow meter.

Chaudhry, M. H. (2014). *Applied Hydraulic Transients,* 3rd ed. Springer, New York, NY.

Chib, S. and E. Greenberg (1995). Understanding the metropolis-hastings algorithm. *The american statistician 49*(4), 327–335.

Ching, J. and J. Beck (2004). Bayesian analysis of the phase ii iasc–asce structural health monitoring experimental benchmark data. *Journal of Engineering Mechanics 130*(10), 1233–1244.

Chopra, A. K. et al. (2012). *Dynamics of structures*, Volume 4th. Pearson Education.

Daily, J. W., W. Hankey Jr, R. Olive, and J. Jordaan Jr (1955). Resistance coefficients for accelerated and decelerated flows through smooth tubes and orifices. Technical report, Massachusetts Inst of Tech Cambridge.

Das, D. and J. H. Arakeri (1998). Transition of unsteady velocity profiles with reverse flow. *Journal of Fluid Mechanics 374*, 251–283.

Der Kiureghian, A. and O. Ditlevsen (2009). Aleatory or epistemic? does it matter? *Structural Safety 31*(2), 105–112.

Duan, H., S. Meniconi, P. Lee, B. Brunone, and M. S. Ghidaoui (2017). Local and integral energy-based evaluation for the unsteady friction relevance in transient pipe flows. *Journal of Hydraulic Engineering 143*(7), 04017015.

Duan, H.-F., M. Ghidaoui, P. J. Lee, and Y.-K. Tung (2010). Unsteady friction and visco-elasticity in pipe fluid transients. *Journal of hydraulic research 48*(3), 354–362.

Duan, H.-F., M. S. Ghidaoui, P. J. Lee, and Y.-K. Tung (2012). Relevance of unsteady friction to pipe size and length in pipe fluid transients. *Journal of hydraulic engineering 138*(2), 154–166.

Eichinger, P. and G. Lein (1992). The influence of friction on unsteady pipe flow. *Unsteady flow and fluid transients*, 41–50.

Garthwaite, P. H., J. B. Kadane, and A. O'Hagan (2005). Statistical methods for eliciting probability distributions. *Journal of the American Statistical Association 100*(470), 680–701.

Gelman, A., J. B. Carlin, H. S. Stern, and D. B. Rubin (2014). *Bayesian data analysis*, Volume 2. Chapman & Hall/CRC Boca Raton, FL, USA.

Geweke, J. et al. (1991). *Evaluating the accuracy of sampling-based approaches to the calculation of posterior moments*, Volume 196. Federal Reserve Bank of Minneapolis, Research Department Minneapolis, MN, USA.

Ghidaoui, M. S. and A. A. Kolyshkin (2001). Stability analysis of velocity profiles in water-hammer flows. *Journal of Hydraulic Engineering 127*(6), 499–512.

Ghidaoui, M. S. and S. Mansour (2002). Efficient treatment of the vardy–brown unsteady shear in pipe transients. *Journal of Hydraulic Engineering 128*(1), 102–112.

Ghidaoui, M. S., S. G. Mansour, and M. Zhao (2002). Applicability of quasisteady and axisymmetric turbulence models in water hammer. *Journal of Hydraulic Engineering 128*(10), 917–924.

Ghidaoui, M. S., M. Zhao, D. A. McInnis, and D. H. Axworthy (2005). A review of water hammer theory and practice. *Applied Mechanics Reviews 58*(1), 49–76.

Hernandez, E. and P. Nestor (2016). A lower bound for the variance of frequency and damping ratio identified from noisy vibration measurements. *Journal of Structural Control and Health Monitoring 23*(1), 5–19.

Hoffman, M. D. and A. Gelman (2014). The no-u-turn sampler: adaptively setting path lengths in hamiltonian monte carlo. *Journal of Machine Learning Research 15*(1), 1593–1623.

Holmboe, E. and W. Rouleau (1967). The effect of viscous shear on transients in liquid lines. *Journal of Basic Engineering 89*(1), 174–180.

Humar, J. (2012). *Dynamics of structures*. CRC Press.

Jaeger, C. (1948). Water-hammer effets in power conduits: Accidents due to water hammer. *Journal of the Institution of Civil Engineers 29*(4), 334–338.

Jaynes, E. T. (2003). *Probability theory: The logic of science*. Cambridge university press.

Kagawa, T. (1983). High speed and accurate computing method of frequency-dependent friction in laminar pipe flow for characteristics method. *JSME Int. J., Ser. B 49*(447), 2638–2644.

Kalkman, C. J. (1995). Labview: a software system for data acquisition, data analysis, and instrument control. *Journal of clinical monitoring 11*(1), 51–58.

Kapelan, Z. S., D. A. Savic, and G. A. Walters (2007). Calibration of water distribution hydraulic models using a bayesian-type procedure. *Journal of Hydraulic Engineering 133*(8), 927–936.

Karney, B. W. (1990). Energy relations in transient closed-conduit flow. *Journal of Hydraulic Engineering 116*(10), 1180–1196.

Katafygiotis, L. S. and J. L. Beck (1998). Updating models and their uncertainties. ii: Model identifiability. *Journal of Engineering Mechanics 124*(4), 463–467.

Khilqa, S., M. Elkholy, M. Al-Tofan, J. M. Caicedo, and M. H. Chaudhry (2019). Damping in transient pressurized flows. *Journal of Hydraulic Engineering, accepted*.

Kim, S., P. Parhi, H. Jun, and J. Lee (2017). Evaluation of drought severity with a bayesian network analysis of multiple drought indices. *Journal of Water Resources Planning and Management 144*(1), 05017016.

Kita, Y., Y. ADACHI, and K. HIROSE (1980). Periodically oscillating turbulent flow in a pipe. *Bulletin of JSME 23*(179), 656–664.

Kreyszig, E. (2010). *Advanced engineering mathematics*. John Wiley & Sons.

Martins, N. M., A. K. Soares, H. M. Ramos, and D. I. Covas (2016). Cfd modeling of transient flow in pressurized pipes. *Computers & Fluids 126*, 129–140.

Meniconi, S., H. Duan, B. Brunone, M. S. Ghidaoui, P. Lee, and M. Ferrante (2014). Further developments in rapidly decelerating turbulent pipe flow modeling. *Journal of hydraulic engineering 140*(7), 04014028.

Metropolis, N., A. W. Rosenbluth, M. N. Rosenbluth, A. H. Teller, and E. Teller (1953). Equation of state calculations by fast computing machines. *The journal of chemical physics 21*(6), 1087–1092.

Mittal, P. (2010). *Oscillations, waves and acoustics*. IK International Pvt Ltd.

Neal, R. M. et al. (2011). Mcmc using hamiltonian dynamics. *Handbook of Markov Chain Monte Carlo 2*(11).

Nixon, W. and M. S. Ghidaoui (2007). Numerical sensitivity study of unsteady friction in simple systems with external flows. *Journal of Hydraulic Engineering 133*(7), 736–749.

O'Hagan, A. (1998). Eliciting expert beliefs in substantial practical applications. *Journal of the Royal Statistical Society: Series D (The Statistician) 47*(1), 21–35.

Pearsall, I. (1965). Paper 2: The velocity of water hammer waves. In *Proceedings of the Institution of Mechanical Engineers, Conference Proceedings*, Volume 180, pp. 12–20. SAGE Publications.

Pezzinga, G. (2000). Evaluation of unsteady flow resistances by quasi-2d or 1d models. *Journal of Hydraulic Engineering 126*(10), 778–785.

Pezzinga, G. and P. Scandura (1995). Unsteady flow in installations with polymeric additional pipe. *Journal of Hydraulic Engineering 121*(11), 802–811.

Plant, H., M. Group, and I. Pearsall (1963). Comparative experiments on surge tank performance. *Proceedings of the Institution of Mechanical Engineers 177*(1), 951–971.

Pothof, I. (2008). A turbulent approach to unsteady friction. *Journal of Hydraulic Research 46*(5), 679–690.

Poulakis, Z., D. Valougeorgis, and C. Papadimitriou (2003). Leakage detection in water pipe networks using a bayesian probabilistic framework. *Probabilistic Engineering Mechanics 18*(4), 315–327.

Puust, R., Z. Kapelan, D. Savic, and T. Koppel (2008). Probabilistic leak detection in pipe networks using the scem-ua algorithm. In *Water Distribution Systems Analysis Symposium 2006*, pp. 1–12.

Ramos, H., D. Covas, A. Borga, and D. Loureiro (2004). Surge damping analysis in pipe systems: modelling and experiments. *Journal of hydraulic Research 42*(4), 413–425.

Reddy, P., W. F. Silva-Araya, and M. Hanif Chaudhry (2011). Estimation of decay coefficients for unsteady friction for instantaneous, acceleration-based models. *Journal of Hydraulic Engineering 138*(3), 260–271.

Schohl, G. (1993). Improved approximate method for simulating frequency-dependent friction in transient laminar flow. *Journal of Fluids Engineering 115*(3), 420–424.

Silva-Araya, W. (1993). *Energy Dissipation in Transient Flow*. Ph. D. thesis, Washington State University.

Silva-Araya, W. F. and M. H. Chaudhry (1997). Computation of energy dissipation in transient flow. *Journal of Hydraulic Engineering 123*(2), 108–115.

Sonin, A. A. (2001). The physical basis of dimensional analysis. *Department of Mechanical Engineering, MIT, Cambridge, MA*, 1–57.

Storli, P.-T. and T. K. Nielsen (2010). Transient friction in pressurized pipes. i: Investigation of Zielke's model. *Journal of Hydraulic Engineering 137*(5), 577–584.

Storli, P.-T. and T. K. Nielsen (2011). Transient friction in pressurized pipes. ii: Two-coefficient instantaneous acceleration–based model. *Journal of Hydraulic Engineering 137*(6), 679–695.

Suo, L. and E. Wylie (1989). Impulse response method for frequency-dependent pipeline transients. *Journal of fluids engineering 111*(4), 478–483.

Tanner, M. A. and W. H. Wong (1987). The calculation of posterior distributions by data augmentation. *Journal of the American statistical Association 82*(398), 528–540.

Taylor, J. (1997). *Introduction to error analysis, the study of uncertainties in physical measurements*, Volume 1.

Thyer, M., B. Renard, D. Kavetski, G. Kuczera, S. W. Franks, and S. Srikanthan (2009). Critical evaluation of parameter consistency and predictive uncertainty in hydrological modeling: A case study using bayesian total error analysis. *Water Resources Research 45*(12).

Tijsseling, A. (1996). Fluid-structure interaction in liquid-filled pipe systems: a review. *Journal of Fluids and Structures 10*(2), 109–146.

Trikha, A. K. (1975). An efficient method for simulating frequency-dependent friction in transient liquid flow. *Journal of Fluids Engineering 97*(1), 97–105.

Vardy, A. and J. Brown (1996). On turbulent, unsteady, smooth-pipe friction. In *Bhr Group Conference Series Publication*, Volume 19, pp. 289–312. Mechanical Engineering Publications Limited.

Vardy, A. and J. Brown (2003). Transient turbulent friction in smooth pipe flows. *Journal of Sound and Vibration 259*(5), 1011–1036.

Vardy, A. and J. Brown (2004). Transient turbulent friction in fully rough pipe flows. *Journal of Sound and Vibration 270*(1-2), 233–257.

Vardy, A. E. and J. M. Brown (2010). Evaluation of unsteady wall shear stress by zielkeâĂŹs method. *Journal of Hydraulic Engineering 136*(7), 453–456.

Vardy, A. E. and K.-L. Hwang (1991). A characteristics model of transient friction in pipes. *Journal of Hydraulic Research 29*(5), 669–684.

Vardy, A. E. and K.-L. Hwang (1993). A weighting function model of transient turbulent pipe friction. *Journal of Hydraulic research 31*(4), 533–548.

Vítkovskỳ, J., M. Lambert, A. Simpson, and A. Bergant (2000). Advances in unsteady friction modelling in transient pipe flow. In *The 8th International Conference on Pressure Surges*, pp. 471–482.

Vítkovskỳ, J. P., A. Bergant, A. R. Simpson, and M. F. Lambert (2006). Systematic evaluation of one-dimensional unsteady friction models in simple pipelines. *Journal of Hydraulic Engineering 132*(7), 696–708.

Weinerowska-Bords, K. (2015). Alternative approach to convolution term of viscoelasticity in equations of unsteady pipe flow. *Journal of Fluids Engineering 137*(5), 054501.

Zarzycki, Z. (1994). Hydraulic resistance in unsteady liquid flow in closed conduits. *Research Reports of Tech. Univ. of Szczecin* (516).

Zhao, M. and M. Ghidaoui (2004). Review and analysis of 1-d and 2-d energy dissipation models for transient flows. In *International conference on pressure surges*.

Zhao, M. and M. S. Ghidaoui (2003). Efficient quasi-two-dimensional model for water hammer problems. *Journal of Hydraulic Engineering 129*(12), 1007–1013.

Zielke, W. (1968). Frequency-dependent friction in transient pipe flow. *Journal of basic engineering 90*(1), 109–115.

Appendix A

Underdamped Pressure Head Oscillations

Closing or opening a valve in a reservoir-pipeline-valve system results in pressure oscillations at the valve that may be describe as the oscillations of the mass in a spring-mass-damper system. The equation describes these pressure oscillations is derived below. Underdamped equation for pressure oscillations may be written as

$$m\ \ddot{h}(t) + c\ \dot{h}(t) + k\ h(t) = 0 \tag{A.1}$$

where m is mass; h is pressure head oscillation; c is damping constant as a measure of the energy dissipation; t is time and k is spring constant. Let us assume that

$$h = Ae^{rt} \tag{A.2}$$

$$\dot{h} = Are^{rt} \tag{A.3}$$

$$\ddot{h} = Ar^2e^{rt} \tag{A.4}$$

By substituting Eqs. A.2, A.3 and A.3 into Eq. A.1, we obtain

$$mAr^2e^{rt} + cAre^{rt} + kAe^{rt} = 0 \tag{A.5}$$

$$Ae^{rt}\left(mr^2 + cr + k\right) = 0 \tag{A.6}$$

Since $Ae^{rt} \neq 0$, therefore

$$mr^2 + cr + k = 0 \tag{A.7}$$

Dividing Eq.A.7 by m gives

$$r^2 + \frac{c}{m}r + \frac{k}{m} = 0 \tag{A.8}$$

Let us define (Chopra et al., 2012),

$\left(\frac{c}{m}\right) = 2b$, $\left(\frac{k}{m}\right) = \omega_n^2$, $c_{cr} = 2m\omega_n$ and $\zeta = \left(\frac{c}{2m\omega_n}\right)$ lead to $\zeta = \left(\frac{b}{\omega_n}\right)$ leads to $b = \zeta\omega_n$, where c_{cr} is critical damping constant, ζ is damping ratio and ω_n is the natural frequency of the piping system which is equal to $a/(4L)$, in rad/sec. L is the length of the pipe and a is the wave velocity.

The roots of Eq. A.7 are

$$r_1 = \frac{-2b + \sqrt{4b^2 - 4\ \omega_n^2}}{2},\ r_1 = b + \sqrt{b^2 - \omega_n^2} \tag{A.9a}$$

$$r_2 = \frac{-2b - \sqrt{4b^2 - 4\ \omega_n^2}}{2},\ r_2 = b - \sqrt{b^2 - \omega_n^2} \tag{A.9b}$$

when $b^2 < \omega_n^2$, the damping case of the pressure head oscillations is *underdamped* and the roots of the Eq. A.7 are complex numbers; therefore,

$$r_1 = b + \sqrt{b^2 - \omega_n^2}\ i \tag{A.10a}$$

$$r_2 = b - \sqrt{b^2 - \omega_n^2}\ i \tag{A.10b}$$

where i is imaginary number, i.e., $\sqrt{-1}$. Let us define, $\alpha = -b$ and $\beta = \sqrt{\omega_n^2 - b^2}$, then substituting α and β into A.10a and A.10b (Kreyszig, 2010)

$$r_1 = \alpha + \beta\ i \tag{A.11a}$$

$$r_2 = \alpha - \beta\ i \tag{A.11b}$$

The general solution of Eq. A.1 for *underdamped* case

$$h = c_1 e^{(\alpha+\beta i)t} + c_2 e^{(\alpha-\beta i)t} \tag{A.12}$$

where c_1 and c_2 are arbitrary constants. By applying Euler's formula, ($e^{\theta i} = cos\theta + isin\theta$), Eq. A.12 becomes

$$h = c_1 e^{\alpha t}\left(cos\beta t + i\ sin\beta t\right) + c_2 e^{\alpha t}\left(cos\beta t - i\ sin\beta t\right) \tag{A.13a}$$

$$h = e^{\alpha t}\left[\left(c_1 + c_2\right) cos\beta t + \left(c_1 - c_2\right) i\ sin\beta t\right] \tag{A.13b}$$

Let us assume $(c_1 + c_2) = A\ sin\phi$ and $(c_1 - c_2) = A\ cos\phi$ (Mittal, 2010), then

$$h = e^{\alpha t}\left(A\ sin\phi\ cos\beta t + A\ cos\phi\ sin\beta t\right) \tag{A.14}$$

Using trigonometric identities, Eq. 3.13 becomes

$$h = e^{\alpha t}\left\{\frac{A}{2}\left[sin\left(\beta t + \phi\right) + sin\left(\beta t - \phi\right)\right] + \frac{A}{2}\left[sin\left(\beta t + \phi\right) - sin\left(\beta t - \phi\right)\right]\right\} \tag{A.15}$$

Eq. A.15 may be simplified as

$$h = Ae^{-bt} sin\sqrt{\omega_n^2 - b^2}\ t \tag{A.16}$$

Substituting $b = \zeta\omega_n$ into Eq. A.16 gives

$$h = Ae^{-\zeta\omega_n t}\ sin\sqrt{\omega_n^2 - \omega_n^2\zeta^2}\ t \tag{A.17}$$

The term $\sqrt{\omega_n^2 - \omega_n^2\zeta^2} = \omega_d$, where ω_d is damped frequency. Since ζ is small, ω_d may be assumed equal to ω_n (Humar, 2012). Eq. A.17 may be written as

$$h = Ae^{-\zeta\omega_n t}\ sin\left(\omega_n t\right) \tag{A.18}$$

Appendix B

Dimensional Analysis For Damping Ratio

Dimensional analysis is used to find the dimensionless parameter affecting the damping in pressure oscillations. This analysis is shown below.

Assuming the damping ratio is a function of the system characteristics

$$\zeta = \psi\left(L, D, V_o, \mu, \rho, K, E, e, \epsilon, g\right) \tag{B.1}$$

where L is the length and D is the diameter of the pipe; V_o is the initial steady state flow velocity; μ is the dynamic viscosity of the fluid; ρ is the fluid density; ϵ is the absolute roughness of the pipe; K is the bulk modulus of elasticity of the fluid; E is Young modulus of elasticity; and e is the pipe thickness.

$$\psi\left(\zeta, L, D, V_o, \mu, \rho, K, E, e, \epsilon, g\right) = 0 \tag{B.2}$$

The repeating variables are: ρ, V_o, D. The following dimensionless numbers (groups), π, are obtained. It should be mentioned that M, L and T stand for mass, length and time dimensions, respectively.

$$\pi_1 = (\rho)^x (V_o)^y (D)^z (\mu)^{-1} \tag{B.3a}$$

$$\left(ML^{-3}\right)^x \left(LT^{-1}\right)^y (L)^z \left(ML^{-1}T^{-1}\right)^{-1} = M^0L^0T^0 \tag{B.3b}$$

$$x - 1 = 0 \tag{B.3c}$$

$$-3x + y + z + 1 = 0 \tag{B.3d}$$

$$-y + 1 = 0 \tag{B.3e}$$

Solving Eqs. B.3c, B.3d and B.3e

$$\pi_1 = \frac{\rho V_o D}{\mu} = \mathrm{Re}_0 \tag{B.4}$$

where Re_0 is Reynolds number.

$$\pi_2 = (\rho)^x (V_o)^y (D)^z (L)^{-1} \tag{B.5a}$$

$$\left(ML^{-3}\right)^x \left(LT^{-1}\right)^y (L)^z (L)^{-1} = M^0 L^0 T^0 \tag{B.5b}$$

$$x = 0 \tag{B.5c}$$

$$-3x + y + z - 1 = 0 \tag{B.5d}$$

$$-y = 0 \tag{B.5e}$$

Solving Eqs. B.5c, B.5d and B.5e

$$\pi_2 = \frac{D}{L} \tag{B.6}$$

$$\pi_3 = (\rho)^x (V_o)^y (D)^z (g)^{-1} \tag{B.7a}$$

$$\left(ML^{-3}\right)^x \left(LT^{-1}\right)^y (L)^z \left(LT^{-2}\right)^{-1} = M^0 L^0 T^0 \tag{B.7b}$$

$$x = 0 \tag{B.7c}$$

$$-3x + y + z - 1 = 0 \tag{B.7d}$$

$$-y + 1 = 0 \tag{B.7e}$$

Solving Eqs. B.7c, B.7d and B.7e

$$\pi_3 = \frac{V_o^2}{Dg} = \mathrm{Fr}^2 \tag{B.8}$$

where Fr is Froude number.

$$\pi_4 = (\rho)^x (V_o)^y (D)^z (\epsilon)^{-1} \tag{B.9a}$$

$$\left(ML^{-3}\right)^x \left(LT^{-1}\right)^y (L)^z (L)^{-1} = M^0 L^0 T^0 \tag{B.9b}$$

$$x = 0 \tag{B.9c}$$

$$-3x + y + z - 1 = 0 \tag{B.9d}$$

$$-y = 0 \tag{B.9e}$$

Solving Eqs. B.9c, B.9d and B.9e

$$\pi_4 = \frac{\epsilon}{D} \tag{B.10}$$

$$\pi_5 = \zeta \tag{B.11}$$

$$\pi_6 = (\rho)^x (V_o)^y (D)^z (K)^1 \tag{B.12a}$$

$$\left(ML^{-3}\right)^x \left(LT^{-1}\right)^y (L)^z \left(MT^{-2}L^{-1}\right)^1 = M^0L^0T^0 \tag{B.12b}$$

$$x + 1 = 0 \tag{B.12c}$$

$$-3x + y + z - 1 = 0 \tag{B.12d}$$

$$-y - 2 = 0 \tag{B.12e}$$

Solving Eqs. B.12c, B.12d and B.12e give

$$\pi_6 = \frac{K}{\rho V_o^2} \tag{B.13}$$

In the dimensional analysis, K, E, and e represent the wave speed which may expressed as Mach number. Therefore, it is appropriate to consider them in terms of wave velocity, a. The pipe inertia and axial pipe motion are not considered which is acceptable for rigidly anchored piping systems (Tijsseling, 1996), i.e., the effect of E is neglected. This gives the following dimensionless group

$$\pi_6 = (\rho)^x (V_o)^y (D)^z (a)^{-1} \tag{B.14a}$$

$$\left(ML^{-3}\right)^x \left(LT^{-1}\right)^y (L)^z \left(LT^{-1}\right)^{-1} = M^0L^0T^0 \tag{B.14b}$$

$$x = 0 \tag{B.14c}$$

$$-3x + y + z - 1 = 0 \tag{B.14d}$$

$$-y + 1 = 0 \tag{B.14e}$$

Solving Eqs. B.14c, B.14d and B.14e

$$\pi_7 = \frac{V_o}{a} = \mathrm{Ma} \tag{B.15}$$

where Ma is Mach number.

A relationship by using dimensional analysis for the damping ratio may be written as

$$\zeta = \psi \left(\mathrm{Re}_0, \mathrm{Ma}, \frac{\epsilon}{D}, \frac{D}{L}, \frac{{V_o}^2}{Dg}\right) \tag{B.16}$$

The effect of Froude number is insignificant in transient pressurized flow, and is dropped. The relative roughness term is dropped for reasons aforementioned in Chapter 3, section 4. Nonlinear regression analysis is used to show the physical dependence of the non-dimensional numbers derived by using the Buckingham theorem and a nominal expression, which satisfies the absolute significance of the relative magnitude of the π-numbers only if it has the power-law form (Sonin, 2001). To account the effect of each π-number, θ is selected equal to one .

$$\zeta = \theta(\mathrm{Re}_0)^{\theta_1}(\mathrm{Ma})^{\theta_2}\left(\frac{D}{L}\right)^{\theta_3} \tag{B.17}$$

Appendix C

Posterior distributions

In this appendix, the other two trails of the posterior distributions are shown, and distributions of ζ predicted by the model are shown as well.

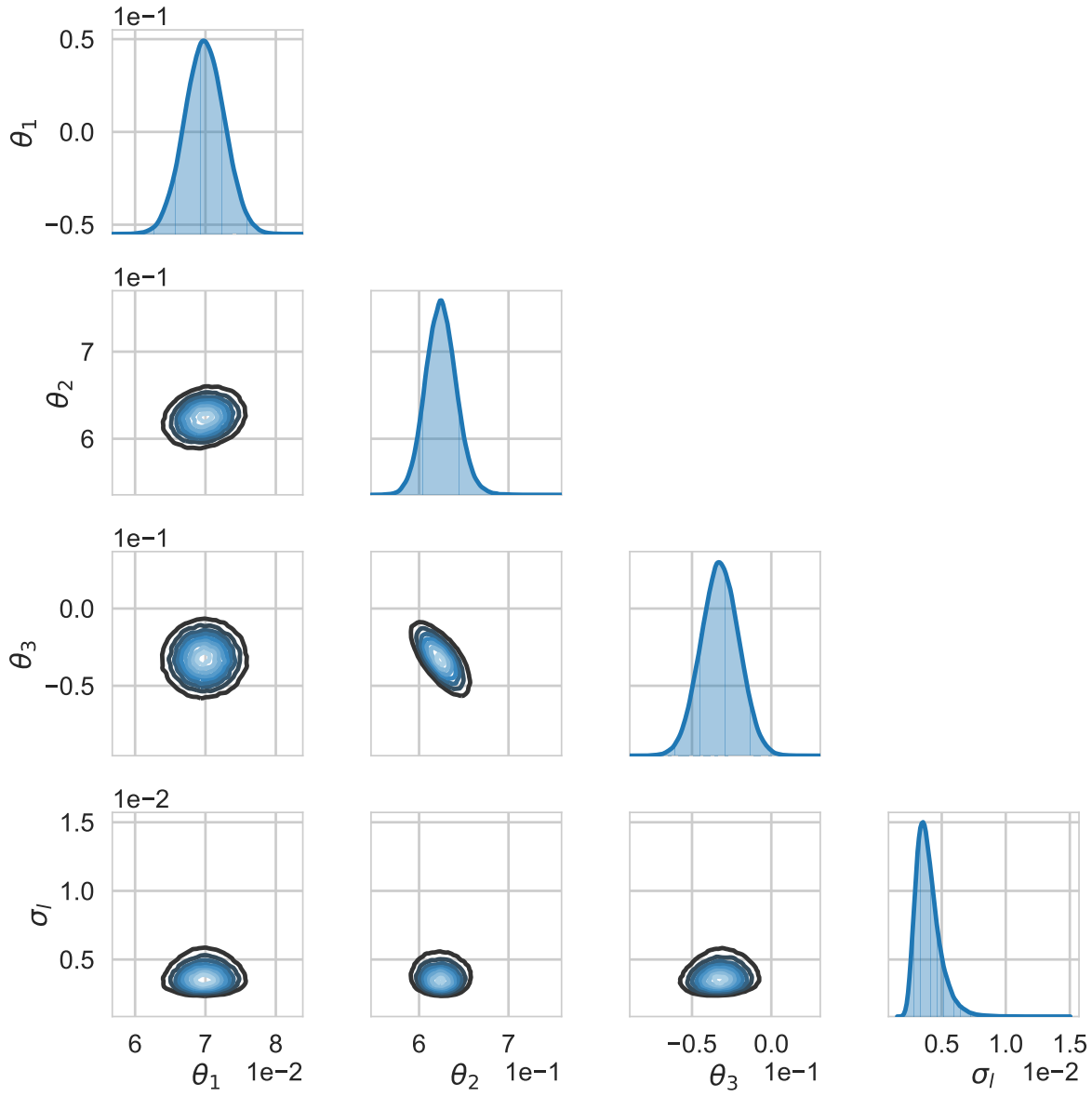

Figure C.1: Posterior distributions of σ_l, θ_1, θ_2 and θ_3 for the first trial.

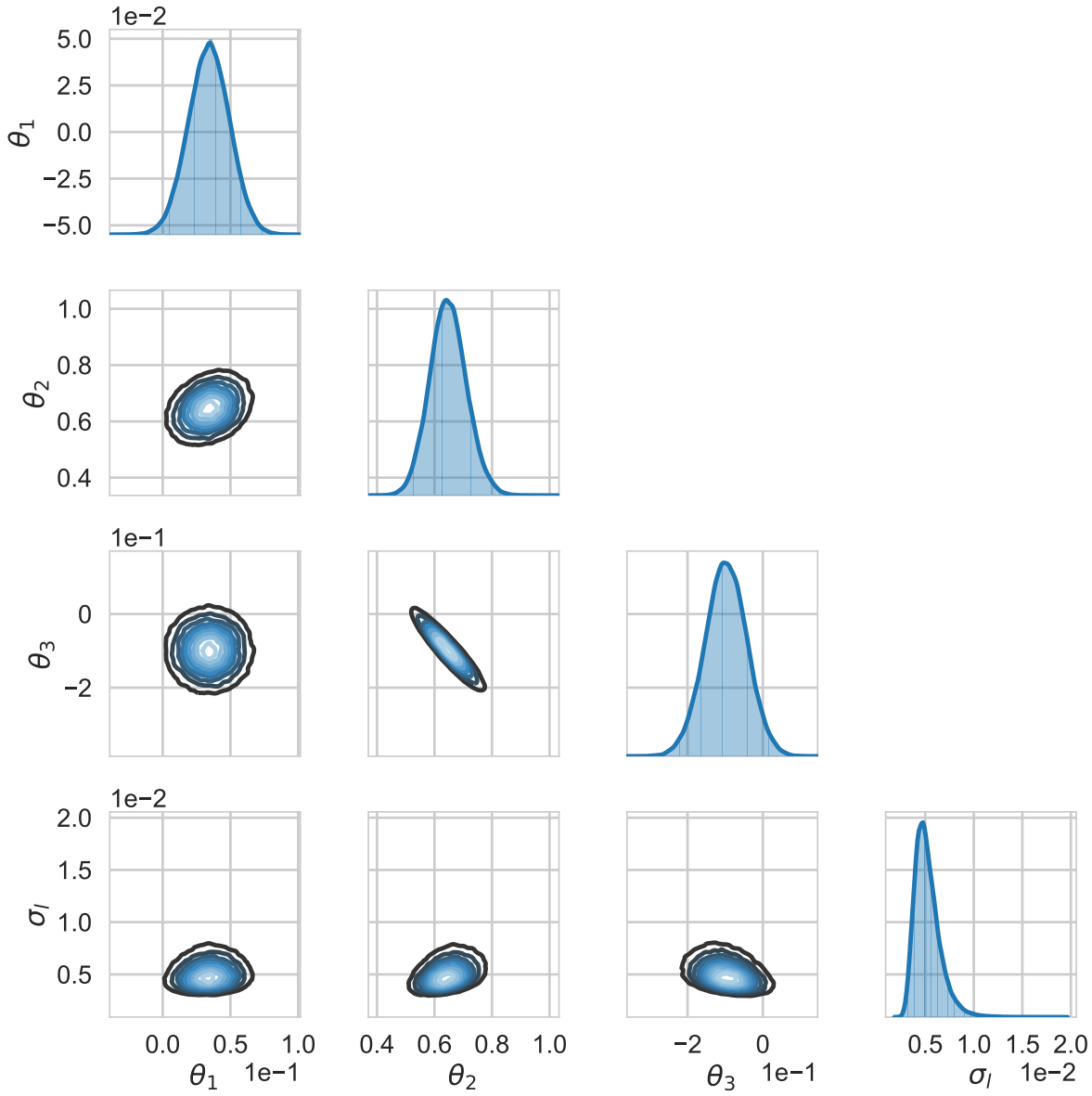

Figure C.2: Posterior distributions of σ_l, θ_1, θ_2 and θ_3 for the third trial.

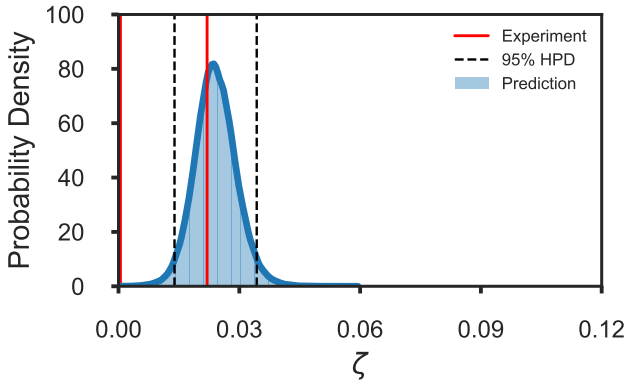

(a)

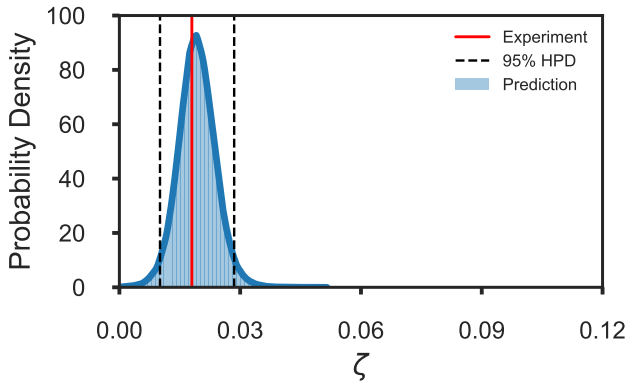

(b)

Figure C.3: Distribution of ζ predicted by the model of first trial: (a) Test 16; (b) Test 15

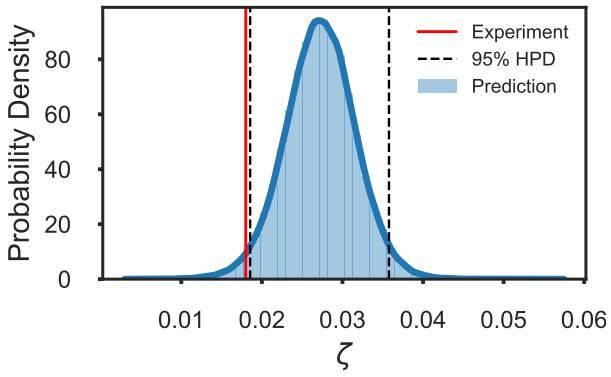

(a)

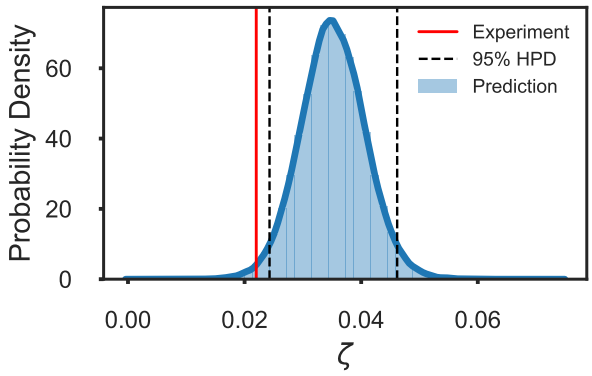

(b)

Figure C.4: Distribution of ζ predicted by the model of second trial: (a) Test 15; (b) Test 16

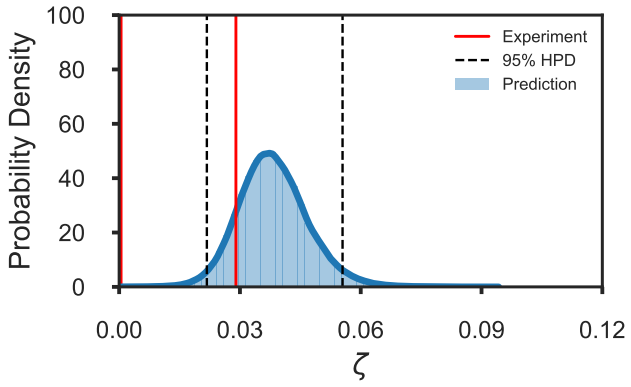

(a)

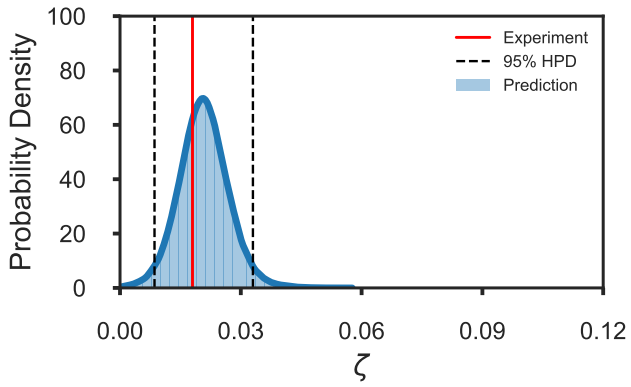

(b)

Figure C.5: Distribution of ζ predicted by the model of third trial: (a) Test 17; (b) Test 15

Appendix D

Permission to Reprint

Permission to reuse your own work

PERMISSIONS <permissions@asce.org>
Mon 08-Apr-19 10:32 AM
To: KHILQA, SAHAD S <skhilqa@email.sc.edu>

Dear Sahad Khilqa,
Thank you for your inquiry. As an original author of an ASCE journal article or proceedings paper, you are permitted to reuse your own content (including figures and tables) for another ASCE or non-ASCE publication (including a dissertation), provided it does not account for more than 25% of the new work. This email serves as permission to reuse your works show below (which are still in production). Please use the assigned DOI (provided below) when referencing the article

- "Damping in Transient Pressurized Flows", *Journal of Hydrologic Engineering*, 10.1061/(ASCE)HY.1943-7900.0001624
- "Uncertainty Quantification for Damping in Transient Pressure Oscillations", *Journal of Water Resources Planning and Management*, 10.1061/(ASCE)WR.1943-5452.0001089

A full credit line must be added to the material being reprinted. For reuse in non-ASCE publica ons, add the words "With permission from ASCE" to your source cita on. For Intranet pos ng, add the following addi onal no ce: "This material may be downloaded for personal use only. Any other use requires prior permission of the American Society of Civil Engineers. This material may be found at [URL/link of abstract in the ASCE Library or Civil Engineering Database]."

Each license is unique, covering only the terms and condi ons specified in it. Even if you have obtained a license for certain ASCE copyrighted content, you will need to obtain another license if you plan to reuse that content outside the terms of the exis ng license. For example: If you already have a license to reuse a figure in a journal, you s ll need a new license to use the same figure in a magazine. You need a separate license for each edi on.

For more informa on on how an author may reuse their own material, please view:
h p://ascelibrary.org/page/informa onforasceauthorsreusingyourownmaterial

Sincerely,

Leslie Connelly
Senior Marke ng Coordinator
American Society of Civil Engineers
1801 Alexander Bell Drive
Reston, VA 20191

PERMISSIONS@asce.org

703-295-6169
Internet: www.asce.org/pubs | www.ascelibrary.org | h p://ascelibrary.org/page/rightsrequests